Renewable and Sustainable Energy Reviews 32 (2014) 347–378

Contents lists available at ScienceDirect

Renewable and Sustainable Energy Reviews

journal homepage: www.elsevier.com/locate/rser

Effect of roughness geometries on heat transfer enhancement in solar thermal systems – A review

Vipin B. Gawande*, A.S. Dhoble, D.B. Zodpe

Department of Mechanical Engineering, Visvesvaraya National Institute of Technology, Nagpur, India

ARTICLE INFO

Article history:
Received 27 February 2013
Received in revised form
6 December 2013
Accepted 4 January 2014
Available online 1 February 2014

Keywords:
Solar air heater
Heat exchangers
Roughness geometry
Thermal performance
Heat transfer
Friction factor

ABSTRACT

The performance characteristics of a solar heater and heat exchangers can be effectively improved by using artificial roughness in different forms, shapes and sizes. Artificial roughness is provided in the form of different geometries such as ribs, dimple shape roughness, wire mesh, baffles, delta winglets etc. To determine the effect of these geometries on thermal performance of solar heaters and heat exchangers, several experimental and numerical studies have been carried out by various researchers. In this paper, an attempt has been made to review various roughness element geometries employed in solar air heaters and heat exchangers in terms of heat transfer, friction factor and flow simulation techniques. Correlations developed for heat transfer and friction factor for different roughness geometries by various investigators in solar air heaters are presente.

Contents

* Corresponding author. Tel.: +91 989 065 9696.
E-mail address: vipingawande@gmail.com (V.B. Gawande).

1364-0321/$ - see front matter © 2014 Elsevier Ltd. All rights reserved.
http://dx.doi.org/10.1016/j.rser.2014.01.024

1. Introduction

In the current era, when there is a continuous demand of energy for the economic progress and industrialization, renewable energy sources are playing vital role in this regard. They are used to design high performance heat transfer systems. Heat transfer enhancement in these thermal systems has numerous applications including cooling of electronics systems, industries, agriculture, space heating etc.

Of the many alternatives, in India solar energy has high solar isolation. It is clean, natural and available in sufficient amount. Devices which are designed on the concept of utilization of this solar energy and works on a principle of conversion of solar energy into thermal energy are heat exchangers and solar air heaters. They are considered as the most cost effective out of all other designed products based on solar energy mainly in commercial and industrial applications. Schematic representation of the solar air heater is shown in Fig. 1.

Solar air heaters are the devices which absorb the incoming solar radiations and convert it into thermal energy at the absorbing surface. The thermal efficiency of solar air heaters has been found to be generally poor because of low convective heat transfer coefficient between the absorber plate and air flowing in the duct [1]. This is because of the formation of laminar viscous sublayer layer which resist the heat transfer. The attempts adopted to enhance the heat transfer includes provision of artificial roughness on the underside of absorber plate in the form of ribs, grooves/dimples, winglets, baffles, twisted tapes, mesh wires, etc.

Artificial roughness is a passive heat transfer enhancement technique by which thermo hydraulic performance of a solar heater can be improved. As the air flows through the duct of a solar air heater, a laminar sub layer is formed over the observer surface that obstruct heat transfer to the flowing air, thereby adversely affecting the thermal performance of the solar air heater. In order to attain higher heat transfer coefficient, it is enviable that flow at the heat transferring surface is made turbulent. However energy for creating such turbulence has to come from fan, which in turn increases the power requirement. So artificially roughened absorber plate is considered to be a good methodology to increase the heat transfer coefficient since it break laminar sub layer in order to reduce thermal resistance. But this also causes simultaneous increase in friction loss in duct. It is therefore desirable to create turbulence in the region very close to the heat transferring surface i.e. in the laminar sub layer only, in order to reduce the friction loss with the application of artificial roughness and power requirement may be lessened. This can be done by keeping the height of the roughness elements to be small in comparison with the duct dimension. Fig. 2 shows the flow behavior in the viscous sublayer region due to presence of repeated roughness elements [6].

The objective of the present paper is

(1) To review the research of different investigators in terms of roughness geometries, which can enhance convective heat transfer in heat exchanger and solar air heaters with minimum increase in friction losses [2].
(2) To classify various types of roughness geometries so that for a specific purpose particular type of geometry can be selected as per the need.
(3) To discuss various types of roughness geometry in terms of geometrical and operating parameters.
(4) To discuss the variation of Nusselt and friction factor dependence with respect to geometrical and operating parameters.
(5) At the same time the various correlations developed by the researchers are also tabulated. The ultimate objective of the paper is to make available a basic platform for further research activities.

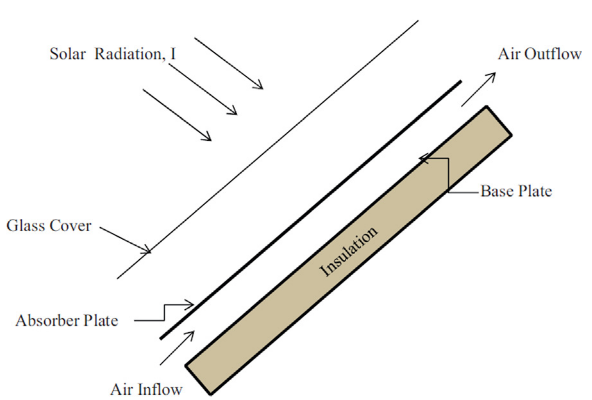


Fig. 1. Schematic diagram of conventional solar heater.

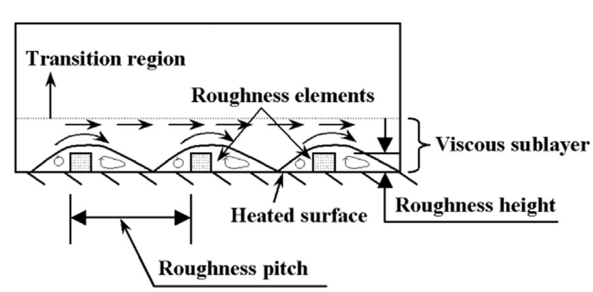


Fig. 2. Effect of roughness elements on flow field.

Nomenclature

C_p	specific heat of air, J/kg K
A_s	surface area of absorber plate, m^2
I	intensity of solar radiations, W/m^2
U_L	overall heat loss coefficient, W/m^{2}K
h	heat transfer coefficient, W/m^{2}K
Q_u	useful heat gain, W
q_u	useful heat flux, W/m^2
m	mass flow rate, kg/s
T_{pm}	mean plate temperature, K
T_{fm}	mean air temperature, K
T_i	fluid inlet temperature, K
T_a	ambient temperature, K
T_o	fluid outlet temperature, K
L	length of duct, m
L_1	inlet length of duct, m
L_2	test length of the duct, m
L_3	outlet length of the duct, m
k	thermal conductivity of air, W/mK
ΔP	pressure drop, Pa
D, D_h	equivalent or hydraulic diameter of duct, m
υ	velocity of air in the duct, m/s
P	pitch, m
P/e	relative roughness pitch
e/D	relative roughness height
g/p	groove position to pitch ratio
d/w	relative gap position
g/e	relative gap width
e^+	roughness Reynolds number
s/e	relative shortway length of mesh
l/e	relative longway length of mesh
l/s	relative length of metal grid
W/w	relative roughness width
e	roughness height
f	friction coefficient of rough surface
f_s	friction coefficient of smooth surface
f_r	friction coefficient of rough surface
BR	blockage ratio
PR	baffle pitch or spacing ratio
X	stream wise Cartesian coordinate (m)
j	Colburn factor
Re	Reynolds number
Re^{Dc}	Reynolds number based on tube outside diameter
R	thermo hydraulic performance factor
R	roughness function
g	heat transfer function

Dimensionless parameters

F_R	heat removal factor
Nu	Nusselt number
Nu_s	Nusselt number for smooth surface
Nu_r	Nusselt number for rough surface
ρ	density of air, kg/m^3

Greek symbols

α, β	angle of attack, degree
$(\tau\alpha)_e$	effective transmittance absorptance product
Φ	wedge angle, degree
δ	thickness of laminar sub layer, m

Abbreviations

VG	vortex generators
CCW	counter clock wise
CW	clock wise

2. Performance analysis of solar air heater

Thermo hydraulic performance of a solar heater helps us to make an efficient system. Thermal performance related with the heat transfer process within the collector and hydraulic performance deals with the pressure drop in the duct. A conventional solar air heater shown in Fig. 1 is considered for detail analysis of thermal and hydraulic performance. Design and construction detail of such type of a conventional system are described by Garg and Prakash [3]. The simplified model as shown in Fig. 3 is consists of wooden rectangular box.

- **Frame** – The frame is generally made of wood or sometimes metal.
- **Matte Black Interior** – All interior surfaces are painted with a heat tolerant matte black paint to absorb as much of the sun's heat as possible.
- **Solar absorber** – This is the most vital part of the unit. The absorber collects the heat which is transferred to air traveling across and through the heated surfaces.
- **Air intake/outlet** – An inlet is provided at the bottom for the entry of the cooler air which after picking up the heat from the absorber, exits the top of the unit. This happens either through a natural process or assisted by a thermostatically-controlled fan.
- **Glazing** – Top surface of the unit is sealed with clear material which receives sun rays which then fall on the solar absorber plate and build up the interior temperature. Typical glazing materials are polycarbonate (Lexan or twinwall type), acrylic, or tempered glass.
- **Insulation** – Insulation is provided on the bottom and side walls to avoid the heat loss from the walls.

3. Thermal performance of solar air heater

Hottel–Whillier–Bliss equation reported by Duffle and Beckman [4] is commonly used to evaluate thermal performance of solar air heater. It is given as

$$Q_u = A_s F_R[I(\tau\alpha)_e - U_L(T_i - T_a)] \tag{1}$$

where
or

$$q_u = Q_u/A_s = F_R[I(\tau\alpha)_e - U_L(T_i - T_a)] \tag{2}$$

The rate of useful energy gain by the flowing air through duct of a solar air heater may also be calculated by using the following

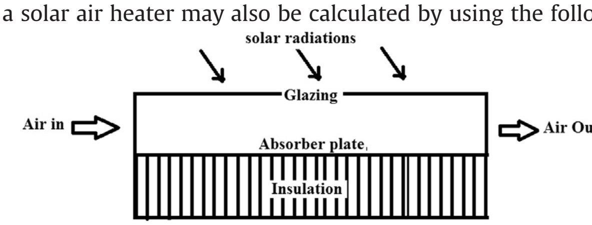


Fig. 3. Simplified model of an air heater.

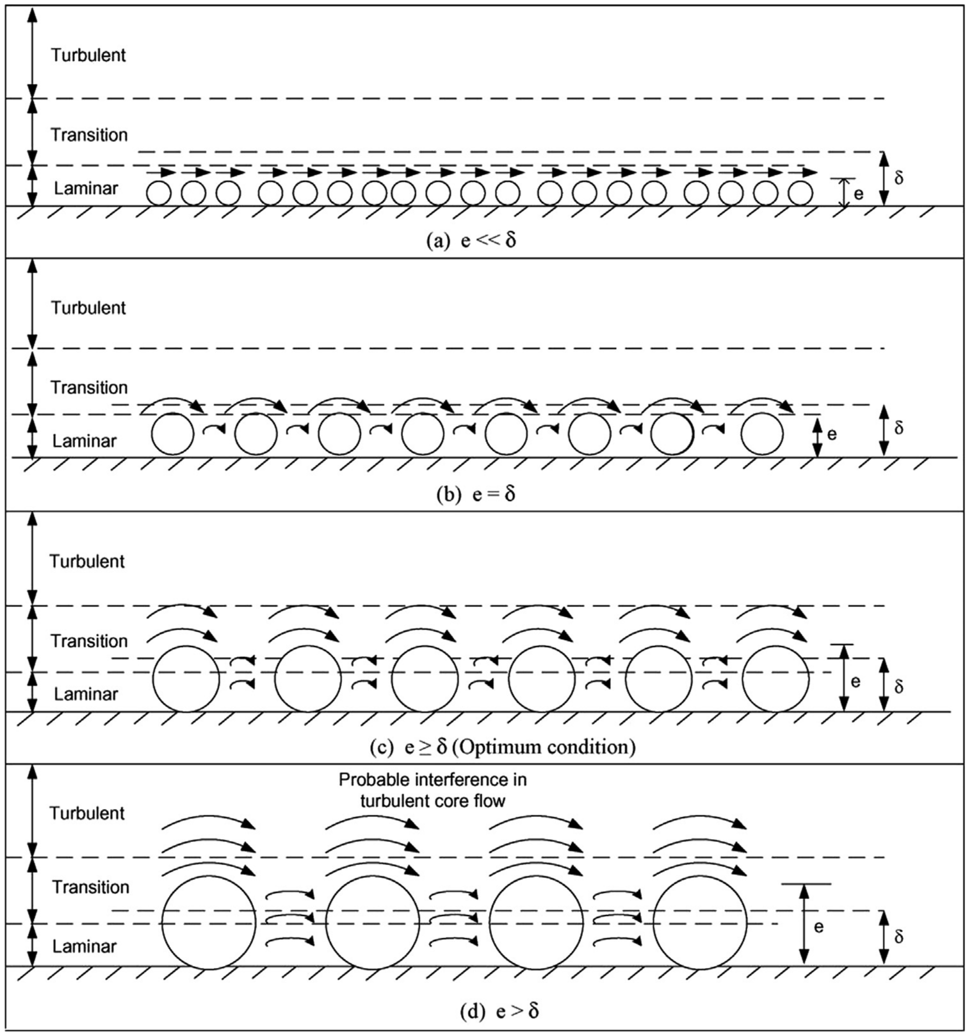


Fig. 4. Effect of rib height on laminar sub layer.

equation:

$$Q_u = mC_pF_R(T_o - T_i) = hA_s(T_{\rm pm} - T_{\rm fm}) \tag{3}$$

As discussed above, heat transfer coefficient (h) is represented in non-dimensional form by using relationship of Nusselt number (Nu) reported by Duffie and Beckman [4].

$$N_u = hL/k \tag{4}$$

Furthermore thermal efficiency of a solar air heater can be expressed by the following equation:

$$\eta_{\rm th} = \frac{q_u}{I} = F_R\left[I(\tau\alpha)_e - \frac{U_L(T_i - T_a)}{I}\right] \tag{5}$$

The above equation shows that the plot between $\eta_{\rm th}$ and parameter $((T_i - T_a)/{\rm I})$ can be approximated by a straight line, of which intercept and slope are given by the values of $F_R\ (\tau\alpha)_e$ and $F_R\ U_L$ respectively.

3.1. Hydraulic performance

Hydraulic performance of a solar air heater concerns with pressure drop (ΔP) in the duct. Pressure drop accounts for energy consumption by fan to propel air through the duct. Pressure drop can be represented in non-dimensional form by using the following relationship of friction factor (f), reported by Frank and Mark [5].

$$f = \frac{(\Delta P)D_h}{2\rho LV^2} \tag{6}$$

3.2. Thermo hydraulic performance

It is desirable that design of a collector should be made in such a way that it should transfer maximum heat energy to the flowing fluid with minimum consumption of fan energy. Therefore in order to analyze overall performance of a solar air heater, thermo hydraulic performance should be evaluated by considering thermal and hydraulic characteristics of the collector simultaneously. The factor is evaluated for various geometries in Section 7.

4. Effect of rib parameters on flow pattern

4.1. Effect of rib

Presence of rib on the underside of the absorber plate creates two flow separation regions, one on each side of the rib. Separation leads to the generation of turbulence and hence the enhancement in heat transfer as well as in the friction losses takes place. Fig. 4 shows the effect of rib height on laminar sub layer explained by Prasad et al. [7]. They reported that,

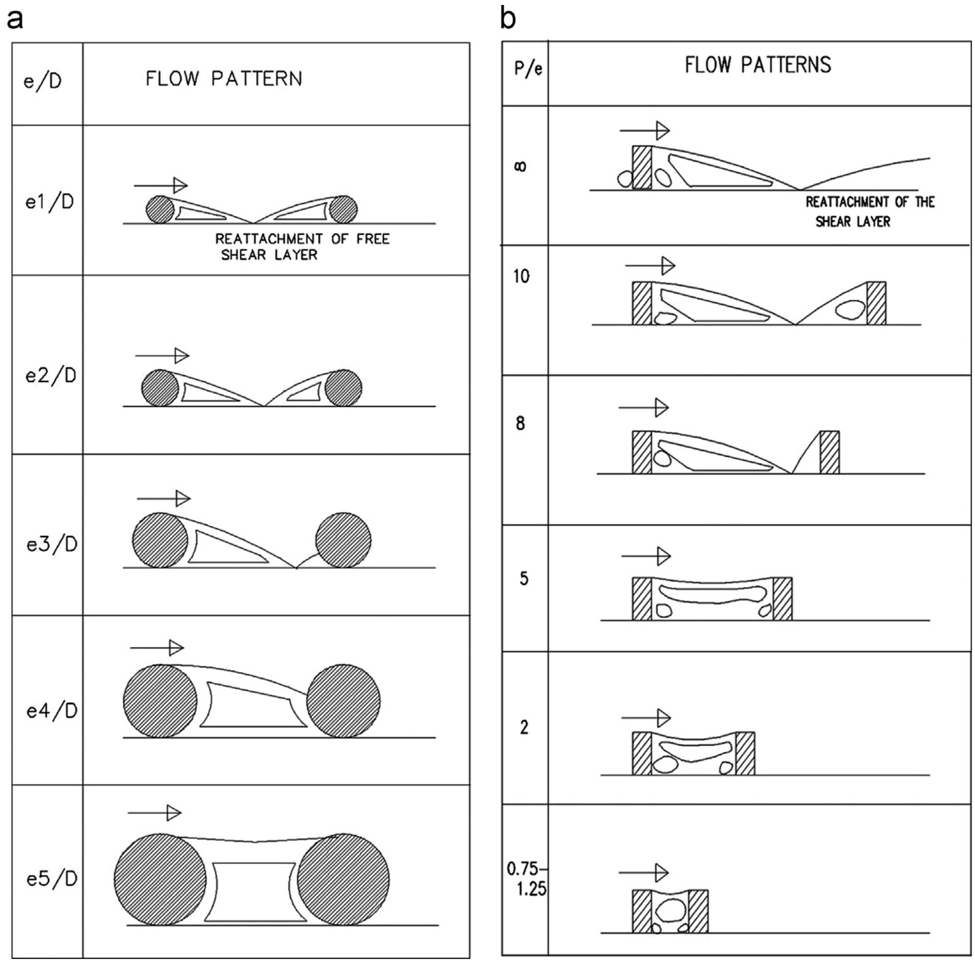


Fig. 5. (a) Effect of rib height and (b) effect of pitch on flow pattern.

(1) If $e \ll \delta$, roughness has no effect
(2) If $e \gg \delta$, roughness has more effect on fluid pressure as compared to heat transfer, due to probable interference of turbulence induced in the already turbulent core.
(3) If $e \geq \delta$, heat transfer has more effect with moderate effect on fluid pressure.

4.2. Effect of rib height and pitch

Flow patterns downstream of a rib with variation in rib height and pitch [8] are shown in Fig. 5. Reattachment of the shear layer does not occur for a pitch ratio of 8 because of flow separation downstream. In the vicinity of a reattachment point, maximum heat transfer occurs. Heat transfer can be similarly enhanced by decreasing the relative roughness pitch (P/e) for fixed relative roughness height (e/D) or by increasing relative roughness height (P/e) for fixed relative roughness pitch (e/D). Relative roughness pitch (P/e) can be increased up to a value of 10, beyond which there is a decrease in heat transfer enhancement.

4.3. Effect of inclination of rib (angle of attack)

Angle attack of the flow with respect to rib position i.e. skewness of the rib towards the flow, is another important vital parameter that influence the pattern of the flow. Angling of the rib produces span wise counter rotating secondary flows which is responsible for significant span wise variation of heat transfer coefficient. The vortices moves along the rib subsequently join the main stream, the fluid entering near the leading end of rib and coming out near the trailing end as shown in Fig. 6. Turbulence developed by moving vortices bring in cooler channel fluid in contact with leading end raising heat transfer rate while the trailing end heat transfer is relatively lower. This effect in strong span wise variation of heat transfer [9].

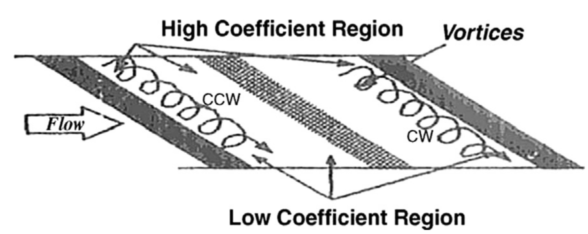


Fig. 6. Effect of inclination of rib.

4.4. Effect of V-shaping of rib

Giving shape to a long, angled rib into v-shape helps in the formation of two leading ends (where heat transfer rate is high) and a single trailing end (where heat transfer is low) resulting in much large area of heat transfer. V-shaped ribs form two secondary flow cells as compared to one in case of a straight angled rib resulting in higher overall heat transfer coefficient in case of v-shaped rib as shown in Fig. 7. V-shaped rib with apex facing downstream has a higher heat transfer as compared to that of with apex facing upstream [9].

As the relative roughness width (W/w) is increased as a result of producing multiple v-ribs heat transfer further increases on account of formation of higher number of leading ends and secondary flow cells as shown in Fig. 8 [10]. According to researchers, there is a formation of two leading ends (where heat transfer rate is high) and a single trailing end (where heat transfer rate is low) as well as two secondary flow cells which promote turbulence mixing which causes increase in heat transfer. Nusselt number increases with increases in relative roughness width (W/w) and attains a maximum value corresponding to relative roughness width (W/w) value of 6 [11].

4.5. Effect of width and position of gap in continuous inclined rib

The inclusion of gap in a rib causes secondary flow along the rib to join the main flow and accelerate it. This in turn helps to energize the retarded boundary layer flow along the surface, resulting in enhancement of heat transfer. Heat transfer enhancement is affected by the position of the gap with respect to leading and trailing edge. Position of the gap near the trailing edge, results in more contribution of secondary flow in energizing the main flow through the gap and recirculation loop in the remaining part of the rib, thereby increasing the heat transfer rate as shown in Fig. 9 [12].

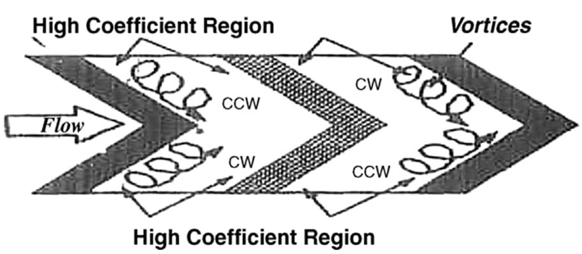


Fig. 7. Effect of V-shaping of rib.

Introduction of a gap in the Multi v-shaped rib allows release of the secondary flow and mix with main flow through the gap as shown in Fig. 10 [10]. This results in its acceleration, which energizes the retarded boundary layer flow along the surface resulting in the increase of the heat transfer through the gap width area behind the ribs [12]. It is also reported that producing a gap near the leading edge does not provide sufficient strength to the secondary flow to energize the main flow passing through the gap and does not lead to increase in heat transfer. Increase in heat transfer is achieved by increasing the relative gap distance, shifting the gap towards the trailing edge. This in turn increases the strength of the secondary flow and thus leads in increase in heat transfer.

4.6. Effect of discretizing of v-shaped ribs

The v-shaped ribs along with staggered rib pieces in between further increase the number and area of heat transfer regions. Additional rib parameters related to the size and positioning of rib pieces (length ratio, B/S, segment ratio, S'/S and staggering ratio, P'/P) with respect to main rib produce complex interaction of secondary flow [13].

4.7. Effect of rib cross section

The level of disturbance in the flow and the size of the separated region are affected by the rib cross-section. Circular cross section had less friction factor as compared to that of rectangular or square cross section ribs. This is due to reduction in the size of the separated region. This causes decrease in inertial

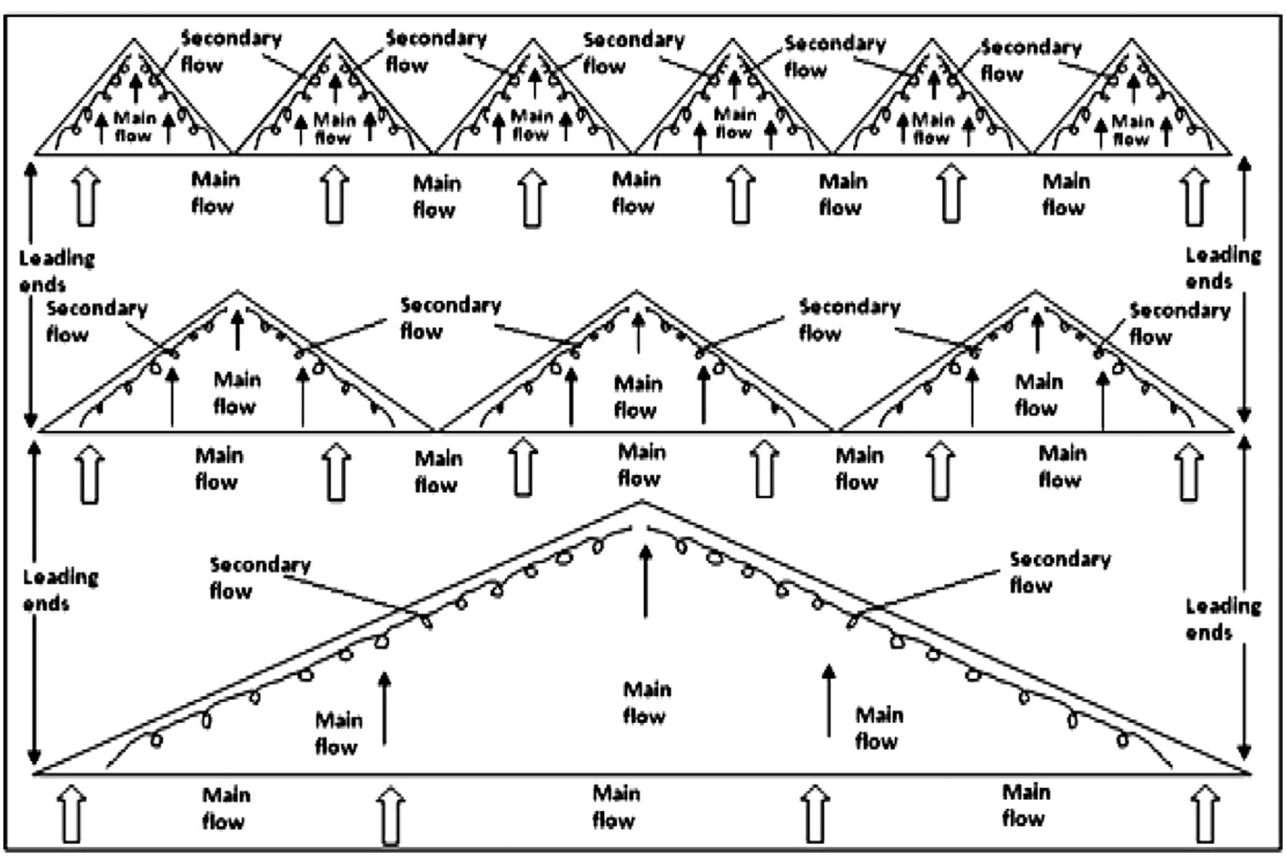


Fig. 8. Flow pattern of secondary flow for multi v-shaped rib.

losses and increase in skin friction, thereby decreasing the friction factor. As the size of the separated region reduces, heat transfer gets affected critically because of decrease in the level of disturbance in flow. The reduction in the heat transfer surface area associated with circular cross section is the cause for Nusselt number decrease [14].

5. Different types of roughness geometries used in solar air heater

Different shapes of roughness elements influencing the heat transfer and friction factor are discussed in the following sections.

5.1. Transverse continuous rib

The application of small diameter wire attached on the underside of absorber plate as a artificial roughness was first introduced by Prasad and Mullick [15] to improve the thermal performance of solar air heater for drying purposes. The experimental study was conducted using the parameters 0.019 as relative roughness height and 12.7 as relative roughness pitch. It is investigated that protruding wires improve plate efficiency factor from 0.63 to 0.72 resulting in 14% improvement in thermal performance.

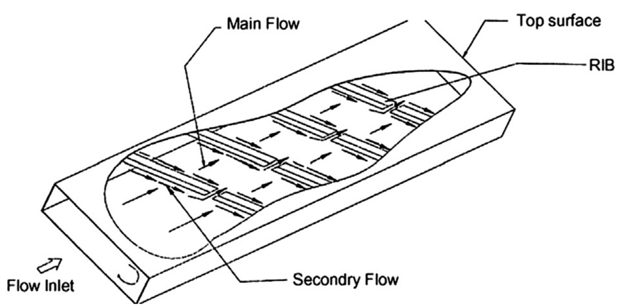


Fig. 9. Effect of width and position of gap in broken inclined rib.

Prasad and Saini [16] investigated the effect of protrusions from underside of absorber surface in the form of small diameter wires on heat transfer and friction factor for fully developed turbulent flow in a solar heater duct. Experimental investigation is carried out using relative roughness pitch of 10, 15 and 20 and relative roughness height of 0.020, 0.027 and 0.033 to detect the effect of height and pitch of roughness on heat transfer and friction. The maximum value of Nusselt number and friction factor is found to be 2.38 and 4.25 respectively at the pitch of 10. The type and orientation of roughness used is shown in Fig. 11.

Kays [17] investigated that fixing small diameter protrusion wires normal to flow direction on the surface of absorber plate helps to break laminar sub layer. It was recommended that protrusion wire diameter of $y^+=50$, spaced 10–20 times diameter and placed within the laminar sub layer are superior to turbulence promoters.

The effect of transverse wire roughness fixed on underside of an absorber plate is studied by Gupta et al. [18]. The experiment was conducted using Reynolds number in the range of 3000–18,000, duct aspect ratio of 6.8–11.5, relative roughness height of 0.018–0.052 at a relative roughness pitch of 10 with a range of roughness Reynolds number between 5 and 70. It has been found that the Staton number increased initially with an increase in Reynolds number up to Reynolds number of 12,000 and then decreases for further increase in Reynolds number.

The effect of transverse wire roughness on heat and fluid flow characteristics for three rectangular solar air heater ducts (two were roughened collectors and one was a plane surface) was investigated by Verma and Prasad [19]. Experiment is carried out using Reynolds number in the range of 5000–20,000 for high duct

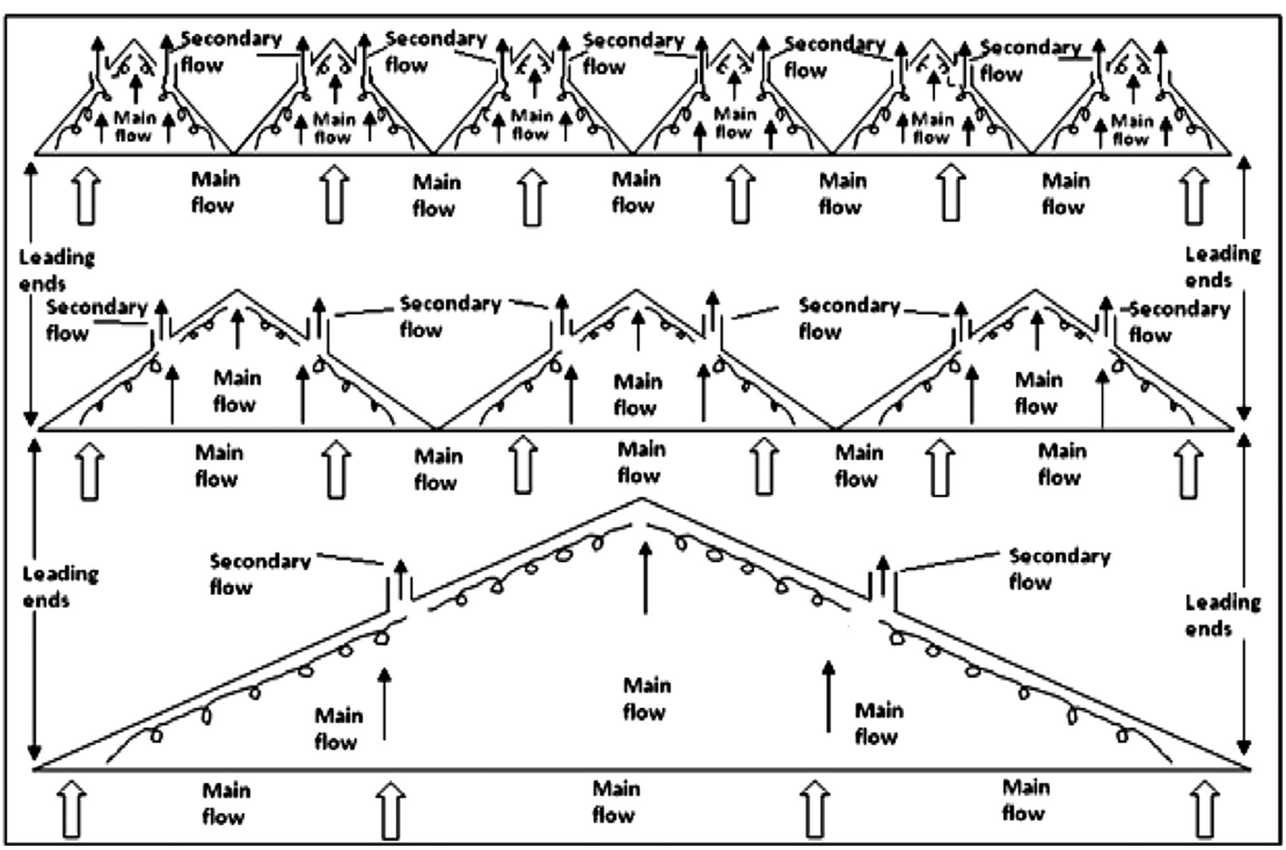


Fig. 10. Flow pattern of secondary flow for multi v-shaped rib with gap.

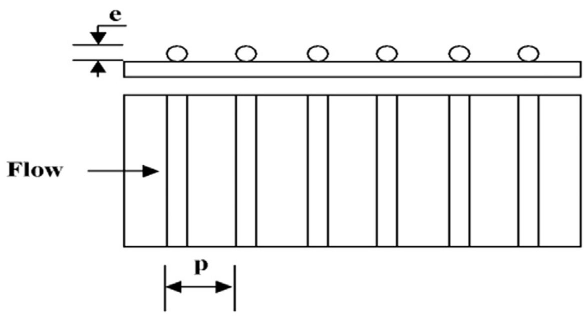


Fig. 11. Transverse rib.

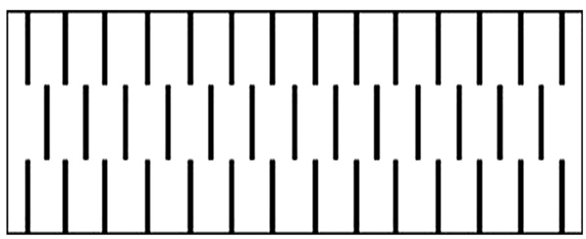


Fig. 12. Transverse broken ribs.

aspect ratio, relative roughness height of 0.01–0.03 at a relative roughness pitch of 10–40 and roughness Reynolds number range of 8–42. An optimum value of about 71% has been reported corresponding to roughness Reynolds number of 24.

5.2. Transverse broken ribs

Sahu and Bhagoria [20] investigated effect of 90° broken transverse ribs on heat and fluid flow characteristics using roughness height of 1.5 mm, duct aspect ratio value of 8, pitch in the range of 10–30 mm and Reynolds number in the range of 3000–12,000. Heat transfer enhancement was reported to be 1.25–1.4 times over smooth duct. From the experiment maximum thermal efficiency was found in the order of 83.5%. Geometry used has been shown in Fig. 12.

5.3. Inclined continuous ribs

Investigators found out that inclined rib gives better heat transfer than transverse ribs due to generation of secondary flow which helps in breaking of the laminar sub layer. Han and Park [21] studied experimentally the effect of inclined ribs in narrow aspect ratio ducts which results in heat transfer enhancement.

The effect of relative roughness height (e/d), inclination of rib with respect to flow direction and Reynolds number (Re) on the thermo hydraulic performance of a roughened solar air heater for transitionally rough flow region ($5 < e^+ < 70$) is studied by Gupta et al. [22]. The experimental result shows that maximum heat transfer and friction factor was in the order of 1.8 and 2.7 times respectively, corresponding to values of angle of inclination as 60° and 70°, respectively. At a relative roughness (e/D) value of 0.023 and Reynolds number value of 14,000, a comparatively best thermo hydraulic performance was reported by investigator. The roughness geometry investigated has been shown in Fig. 13.

An experimental investigation of forced convection heat transfer in a rectangular channel (aspect ratio AR=5) with angled rib turbulators, inclined at 45°, was presented by means of the steady-state liquid crystal thermography by Tanda [81]. To study the effect of rib spacing on the thermal performance of the ribbed

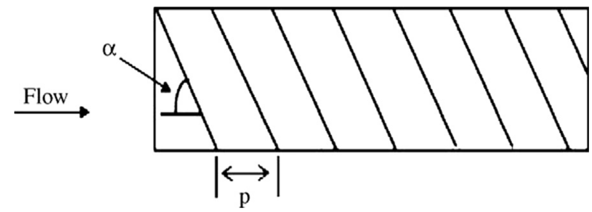


Fig. 13. Inclined continuous ribs.

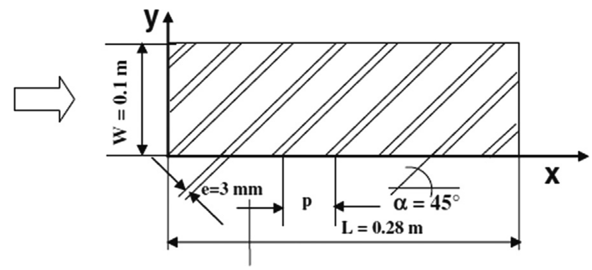


Fig. 14. Geometry of the ribbed heated surface.

channel, the parallel ribs have been installed either onto one wall of the channel (1RW case) or, in-line, onto two opposite walls (2RW case) with a rib pitch-to-height ratio ranging from 6.66 to 20.0. Heat transfer augmentations, relative to the smooth channel with the same mass flow rate, decrease with Re, as typically occurs in rib-roughened channels, and range from 1.6 to 2.25 for the 1 RW case and from 1.85 to 2.55 for the 2RW case. Geometry investigated is shown in Fig. 14.

5.4. Inclined rib with gap

Aharwal et al. [23] studied the effect of width and position of gap in inclined split-ribs having square cross section on heat transfer and friction characteristics of a rectangular air heater duct. The increase in Nusselt number and friction factor was in the range of 1.48–2.59 times and 2.26–2.9 times of the smooth duct respectively for the range of Reynolds numbers from 3000 to 18,000. Corresponding to a relative gap width (g/e) value of 1.0 and relative gap position (d/W) value of 0.25, values of heat transfer, friction factor ratio (f/f_s) and thermo hydraulic performance parameters were found to be maximum. It was investigated that relative gap width beyond 1.0 reduces the flow velocities through the gap and which reduces heat transfer as compared to continuous ribs. If the relative gap width was taken lower than 1.0, then it shrinks the passage for secondary flow release which reduces the turbulence intensity behind the gap and hence reduces heat transfer. The geometry investigated has been shown in Fig. 15.

Cho et al. [24] experimentally investigated the effect of gap in the inclined ribs on heat transfer in square duct with rib to pitch height ratio of 8 and angle of attack of 60°. Experiments were carried out by maintaining the gap width same as the rib width and by varying the gap position over the duct width for parallel and cross rib arrangement on two opposite walls, they investigated that, the inclined rib with a downstream gap shows significant enhancement in heat transfer as compared to that of continuous inclined rib arrangement. The geometry used for study is shown in Fig. 16.

An experimental study has been carried out by Kumar et al. [25] for enhancement of heat transfer coefficient of a solar air heater having roughened air duct provided with artificial roughness in the form 60° inclined discrete rib. The maximum heat transfer enhancement occurs for the relative roughness pitch of 12, relative gap position of 0.35 and relative roughness height of

0.0498. Statistical correlations for Nusselt number and friction factor have been developed as a function of gap position, rib height (or depth), pitch and Reynolds number. These correlations have been found to predict the values of Nusselt number and friction factor with average absolute standard deviation of 3.8% and 3.4%, respectively. The investigated geometry has been shown in Fig. 17.

5.5. Combined inclined and transverse rib

Experimental study on heat transfer and friction characteristics by using a combination of inclined and transverse ribs on the absorber plate of solar air heater was conducted by Varun et al [26]. The best thermal performance was reported for relative roughness pitch value of 8. The investigated geometry is shown in Fig. 18.

5.6. V-shaped ribs

Experiments were conducted by Lau et al. [27–29] to study the effect of discrete V-shaped ribs on turbulent heat transfer and friction for fully developed flow of air in a square channel. They found that the average Staton number for the inclined 45° and 60° ribs was 20–35% higher than in the 90° full rib cases. Fig. 19 shows the typical rib configuration.

Han et al. [30] studied the effect of parallel and V-shaped staggered discrete ribs and found out that 60° staggered discrete V-shaped ribs provide higher heat transfer than that for the parallel discrete ribs.

Momin et al. [31] studied the effect of V-shaped roughness as shown in Fig. 20, on heat transfer and friction characteristics of solar air heater duct. It was investigated that V-shape ribs with an angle of attack of 60° enhanced Nusselt number by 1.14 and 2.30 times and friction factor by 2.30 and 2.83 times over inclined ribs and smooth plate respectively.

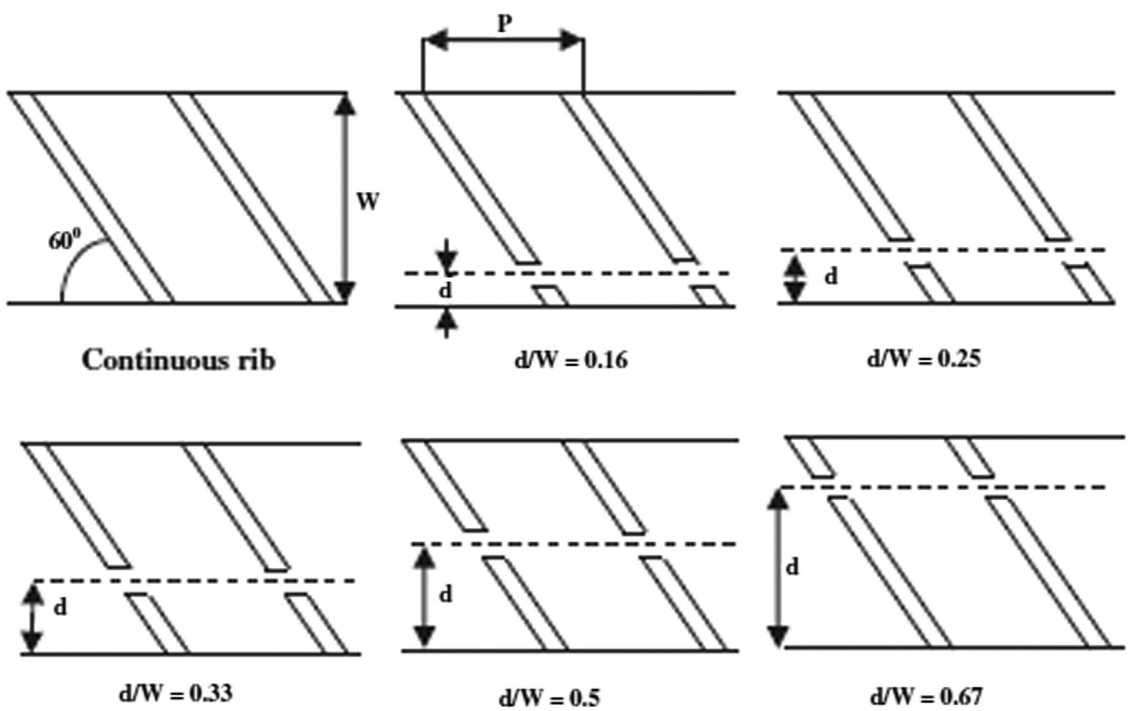


Fig. 15. Inclined ribs with gap.

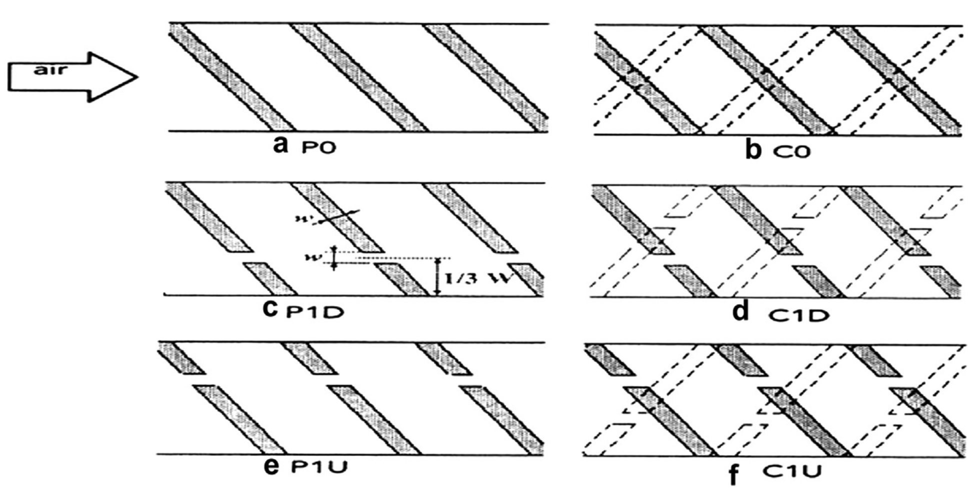


Fig. 16. Rib arrangement with a gap.

The heat and fluid flow characteristics of rectangular duct having its one broad wall heated and roughened with periodic 'discrete V-down rib' are experimentally investigated by Singh et al. [32]. As Reynolds number is increased, the Nusselt number increase is more for discrete V-down rib as compared to continuous V-down rib. This is probably due to increase in local Nusselt number downstream of gap caused by increased flow velocity through the gap. It is observed that at all Reynolds number, the Nusselt number increases with increase in relative roughness pitch (P/e) up to the value of 8.0 and then reduces as (P/e) is increased further. It is observed that at all Reynolds number, the Nusselt number increases as relative gap width (g/e) is increased from 0.5 to 1.0 and thereafter it decreases as (g/e) is increased further. The value of Nusselt number is found to be highest at angle of attack (α)$=60^{\circ}$. Also maximum value of Nusselt number is recorded at relative gap position (d/w) of 0.65. The investigated geometry has been shown in Fig. 21.

Comparison of thermal performance of roughened absorber plate fixed with staggered discrete V-apex (up and down) was done by Maluwork et al. [33,34]. The increase of relative roughness length ratio in the range of 3–7, increases Staton number. Boosting in Staton number ratio was found to be of the order of 1.32–2.47. Rib geometry used is shown in Fig. 22.

Karwa et al. [35] had conducted experimental study on heat transfer and friction in a high aspect ratio duct with transverse, inclined, V-up continuous and V-down continuous, V-up discrete ribs and V-down discrete ribs. He investigated that enhancement in Staton number over smooth duct was found to be 65–90%,87–112% 102–137%, 110–147%, 93–134%, 102–142% respectively. The friction factor ratio for V-up continuous and V-down continuous, V- up discrete ribs and V-down discrete ribs was found to be 3.92, 3.65, 2.47 and 2.58 respectively. Roughness geometry investigated shown in Fig. 23.

An experimental investigation had been carried out by Hans et al. [11] to study the effect of multiple v-rib roughness as shown in Fig. 24 on heat transfer coefficient and friction factor in an artificially roughened solar air heater duct. A maximum enhancement of Nusselt number and friction factor due to presence of such an artificial roughness has been found to be 6 and 5 times, respectively, in comparison to the smooth duct for the range of parameters considered. The maximum heat transfer enhancement has been found to occur for a relative roughness width (W/w) value of 6, while friction factor attains maximum value for relative roughness width (W/w) value of 10. It has also been found that

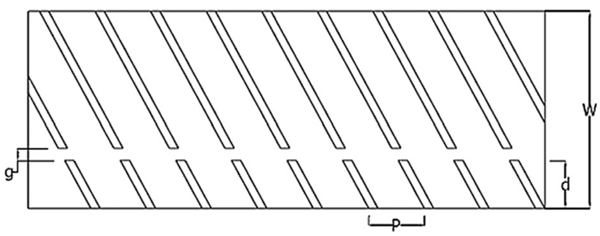


Fig. 17. Geometry of 60° inclined discrete rib roughness.

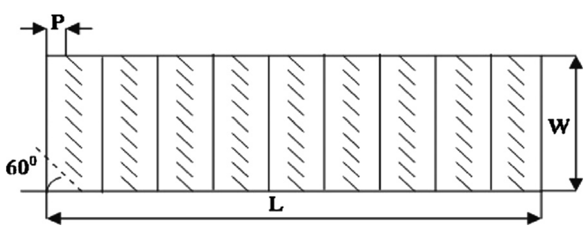


Fig. 18. Combined inclined and transverse rib.

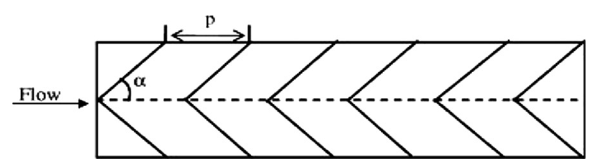


Fig. 20. Roughened absorber plate with V-shaped ribs.

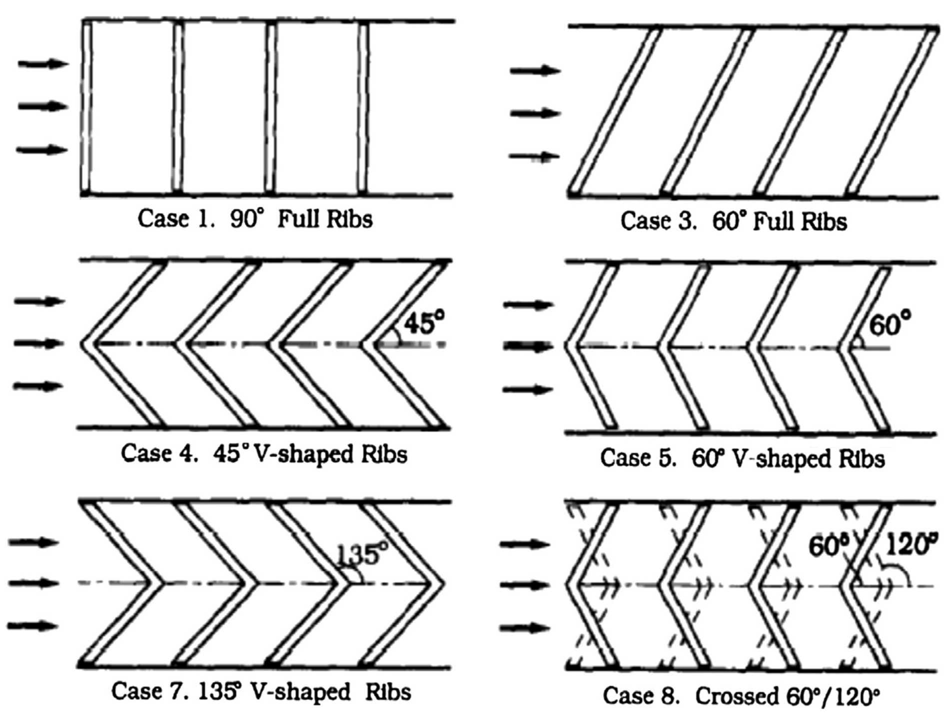


Fig. 19. Typical rib configuration.

Nusselt number and friction factor attain maxima corresponding to angle of attack (a) value of 60° and a relative roughness pitch (*P*/*e*) value of 8.

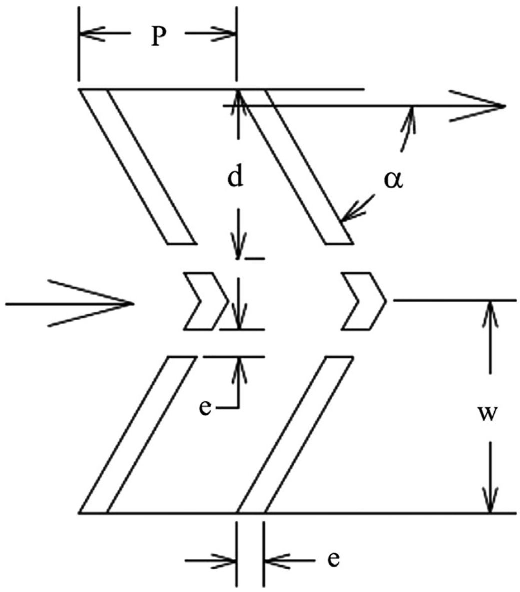


Fig. 21. Discrete V-down rib arrangement.

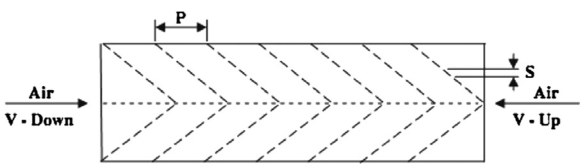


Fig. 22. Discrete V-shaped ribs.

5.7. Wedged-shaped transverse ribs

Bhagoria et al. [36] experimentally investigated the effect of wedge shaped transverse repeated rib roughness on one broad heated wall of solar air heater duct on fluid flow characteristics. The experiment includes the Reynolds number range from 3000 to 18,000, relative roughness pitch 12.12 to 60.17, relative roughness height 0.015–0.033. Maximum Nusselt number was obtained at a relative pitch of 7.57 and decreases further with the increase of pitch from 7.57 to 12.12. The friction factor keeps decreasing as the relative roughness pitch increases. A maximum improvement of heat transfer occurs at a wedge angle of about 10° whereas Nusselt number decreases on either side of this wedge angle. The friction factor increases as the wedge angle increases. The investigated geometry has been shown in Fig. 25.

5.8. Combination of different rib roughness elements

The effect of relative roughness pitch (*P*/*e*), relative roughness height (*e*/*D*) and relative groove position (*g*/*P*) on the heat transfer coefficient and friction factor has been studied experimentally by Jaurker et al. [37] using rib-grooved roughness. Investigation reveals that Nusselt number increases up to 2.7 times while friction factor yield up to 3.6 times as compared to smooth absorber plate. The maximum enhancement in heat transfer and friction factor comes about for a relative roughness pitch (*P*/*e*) of about 6 and relative groove (*g*/*P*) value of 0.4. The higher turbulence intensity formed due to vortices induced in and around the grooves, found to be responsible for higher heat transfer rates. The geometry investigated has been shown in Fig. 26.

Layek et al. [38] experimentally investigated heat transfer and friction factor characteristics of repeated integral transverse chamfered rib groove arrangement on absorber plate of a solar air

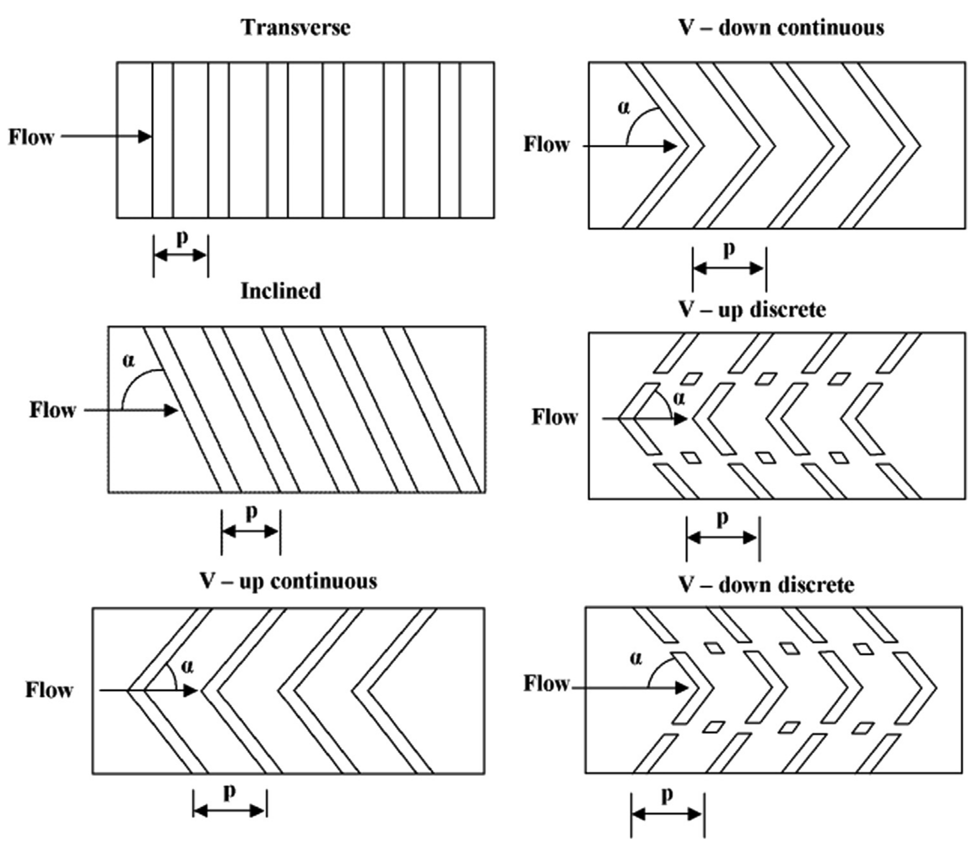


Fig. 23. Roughness geometry.

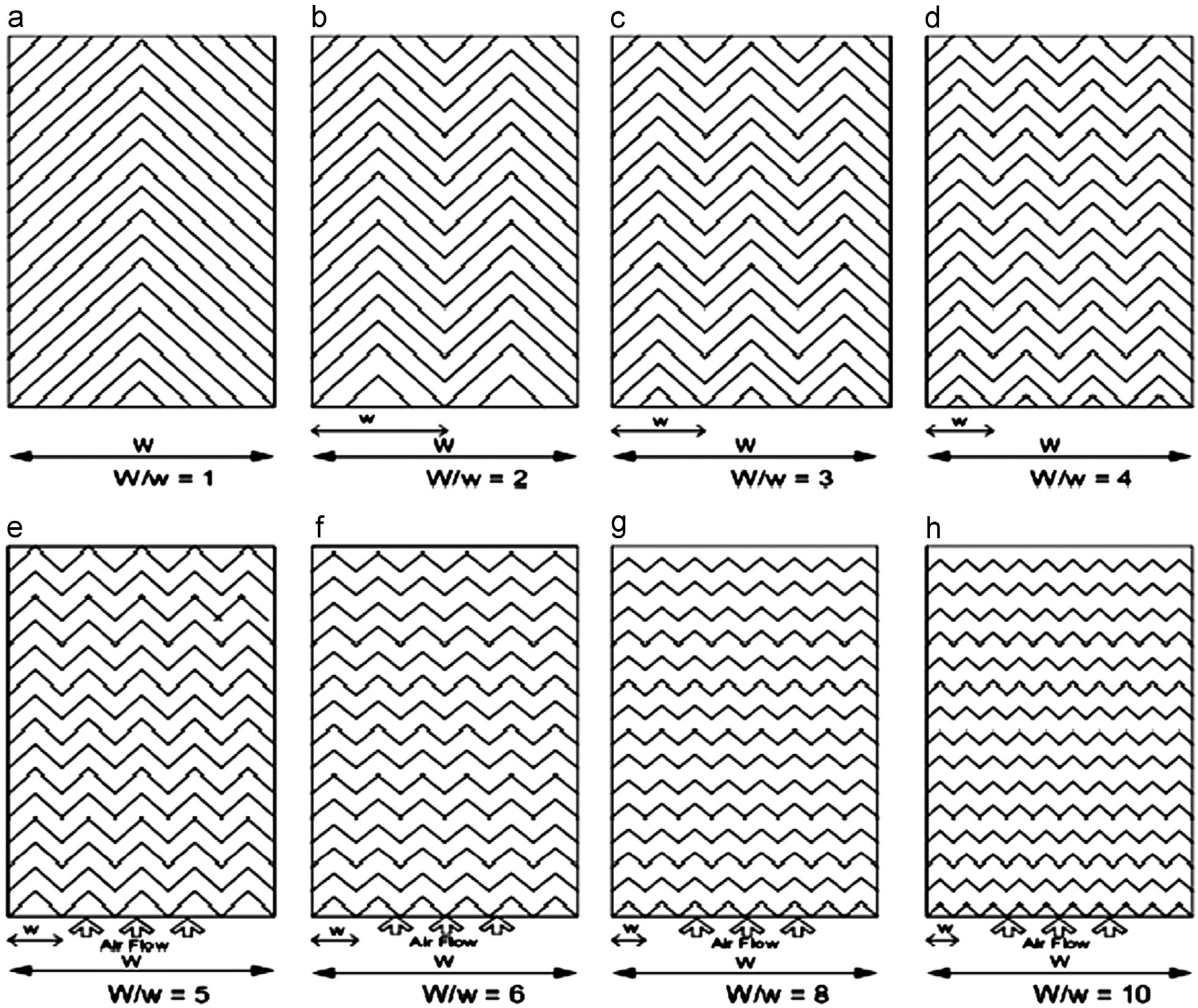


Fig. 24. Roughened absorber plates.

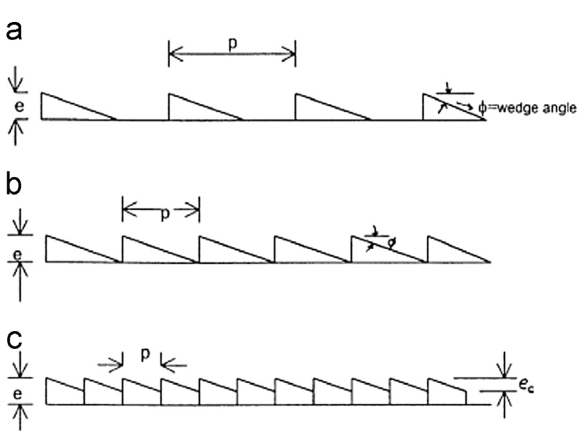


Fig. 25. Wedged shaped ribs.

heater as shown in Fig. 27. Experiments were carried out using four relative groove positions (g/P) values of 0.3–0.6, relative roughness height of 0.022–0.04, chamfer angle of 5–30° and Reynolds number range of 3000–21,000. The experimental result shows that Nusselt number and friction factor increased by 3.24 times and 3.78 times respectively as compared to smooth duct.

5.9. Chamfered ribs

Karwa et al. [39] experimentally studied heat transfer and friction characteristics for rectangular ducts, having aspect ratio (W/H) in the range of 4.8–12, roughened with repeated integral chamfered ribs as shown in Fig. 28. At chamfer angle value of 15°, maximum value was attained by Staton number and friction factor. It was studied that, Staton number decreased while friction factor increased as the aspect ratio (W/H) was increased.

5.10. Expanded metal mesh ribs or wire mesh

Saini and Saini [40] experimentally studied effect of expanded metal mesh as roughness geometry as shown in Fig. 29. It was investigated that enhancement of heat transfer coefficient and friction factor of the order of 4 and 5 times over the smooth duct corresponding to the angle of attack of 61.9° and 72° respectively was obtained.

A parametric study of artificial roughness geometry of expanded metal mesh type in the absorber plate of solar air heater duct has been carried out by Gupta et al. [41] as shown in Fig. 29. The performance evaluation in terms of energy augmentation ratio (*EAR*), effective energy augmentation ratio (*EEAR*) and exergy augmentation ratio (*EXAR*) has been carried out for various values of Reynolds number (Re) and roughness parameters of expanded

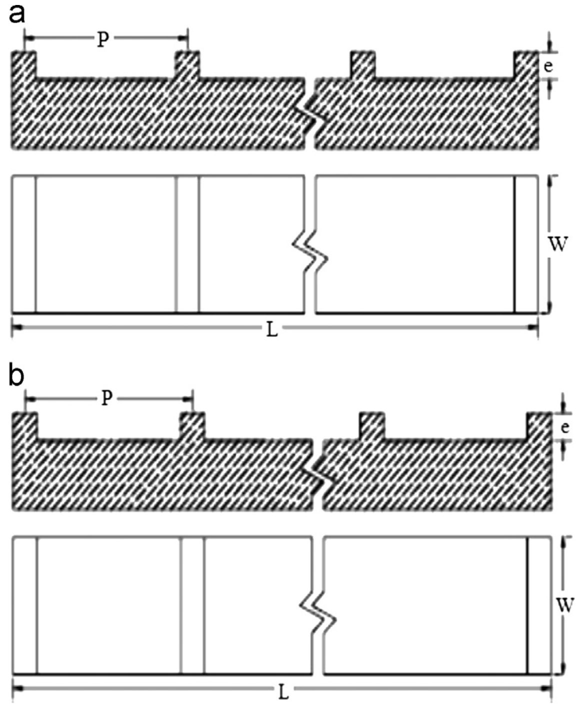


Fig. 26. (a) Rib roughness geometry and (b) rib groove geometry.

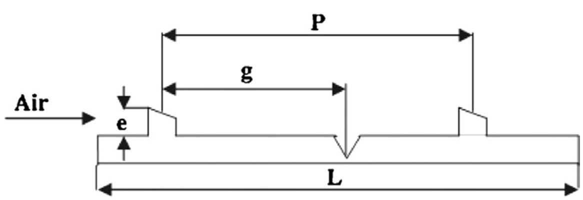


Fig. 27. Chamfered rib grooved artificial roughness.

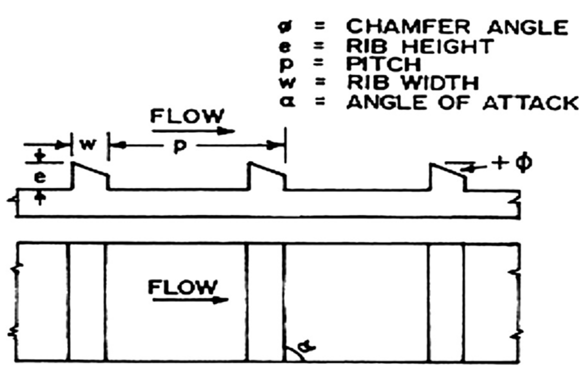


Fig. 28. Chamfered rib geometry.

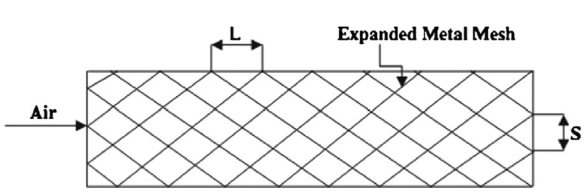


Fig. 29. Expanded metal mesh.

metal mesh roughness geometry in the absorber plate of solar air heater duct. It was investigated that the augmentation ratios decrease at faster rate with Reynolds number in the order of *EAR*, *EEAR* and *EXAR*. It was also studied that augmentation ratios increase with increase in duct depth and intensity of solar radiation. It was apparent that (l/e) of 40 resulted highest EXAR followed by (l/e) of 55.

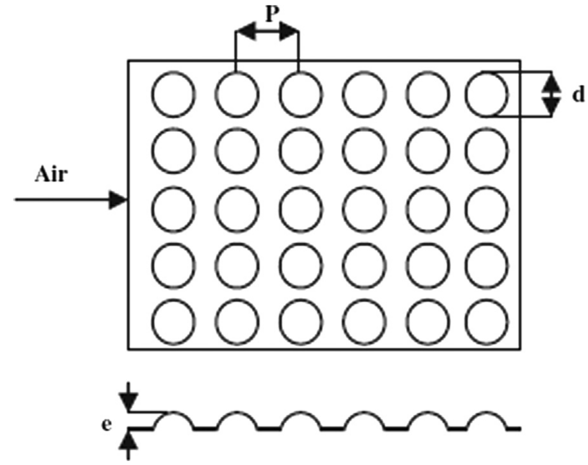


Fig. 30. Dimple shaped ribs.

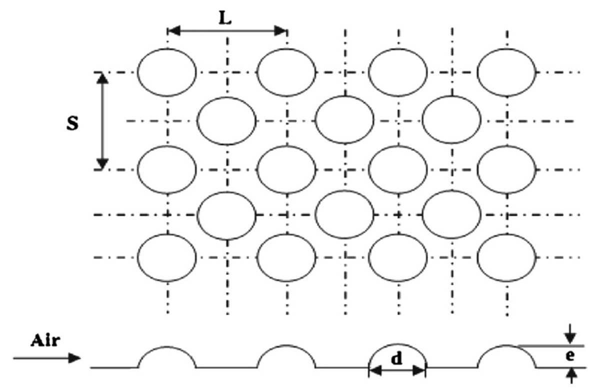


Fig. 31. Dimple protrusion in staggered manner.

Thermal performance of wire-screen metal mesh was experimentally studied by Paswan et al. [42] as artificially roughened on the underside of absorber plate. Thermal performance enhancement of a solar air heater was depends strongly on the diameter of the wire and pitch, mass flow rate, insulation and inlet temperature. It was investigated that decreasing wire pitch, thermal performance of a solar air heater increases.

5.11. Dimple/protrusion shaped geometry

An experimental investigation was conducted by Saini et al. [43] using dimple shaped roughness geometry as shown in Fig. 30 on the underside of absorber plate of the solar air heater duct. The maximum yield in heat transfer was found corresponding to relative roughness height of 0.0379 and relative roughness pitch of 10 and minimum value of friction factor was been found corresponding to relative roughness height of 0.0289 and relative roughness pitch of 10.

An experimental investigation has been carried out by Bhushan et al. [44] for a range of system and operating parameters in order to analyze effect of artificial roughness on heat transfer and friction in solar air heater duct having protrusions as roughness geometry as shown in Fig. 31. Maximum enhancement of Nusselt number and friction factor has been found 3.8 and 2.2 times respectively in comparison to smooth duct for the investigated range of parameters. Maximum enhancement in heat transfer coefficient has been found to occur for relative short way length (S/e) of 31.25, relative long way length (L/e) of 31.25 and relative print diameter (d/D) of 0.294.

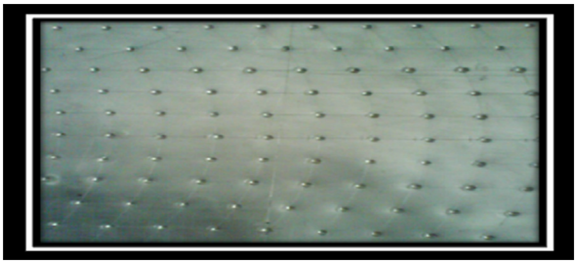


Fig. 32. Roughness geometry.

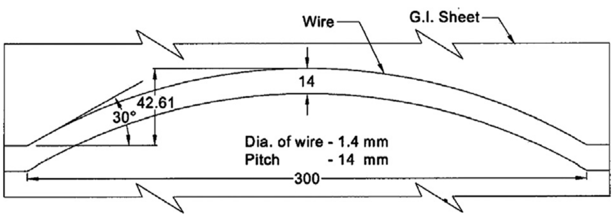


Fig. 33. Arc shape roughness.

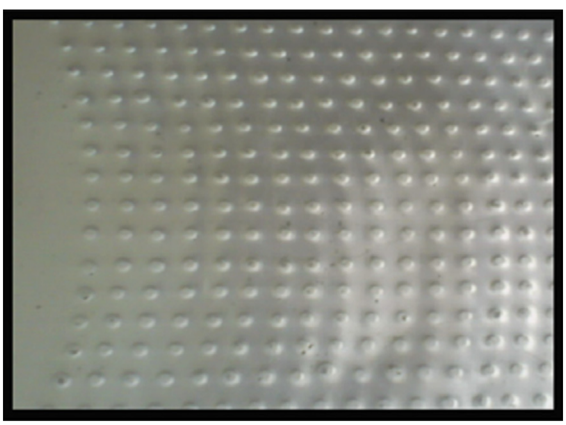


Fig. 34. Roughness geometry.

An experimental investigation has been carried out by Sethi et al. [84] to analyze the effect of artificial roughness on heat transfer and friction characteristics in solar air heater duct with dimple shaped elements arranged in angular fashion (arc) as roughness elements on absorber plate as shown in Fig. 32. The maximum value of Nusselt number has been found corresponding to relative roughness height of 0.036, relative roughness pitch of 10 and arc angle of 60°.

5.12. Arc shaped ribs

An experimental study has been carried out by Saini et al. [45] for enhancement of heat transfer coefficient of a solar air heater having roughened air duct provided with artificial roughness in the form of arc-shape parallel wire as roughness element as shown in Fig. 33. The maximum enhancement in Nusselt number has been investigated as 3.80 times corresponding to the relative arc angle ($\alpha/90$) of 0.3333 at relative roughness height of 0.0422. On the other hand, the increment in friction factor corresponding to these parameters has been observed 1.75 times only.

An experimental investigation has been carried out by Yadav et al. [83] to study the effect of heat transfer and friction characteristics of turbulent flow of air passing through rectangular duct which is roughened by circular protrusions arranged in angular arc fashion as shown in Fig. 34. The investigations reported the maximum enhancement in heat transfer and friction factor as 2.89 and 2.93 times as compared with smooth duct.

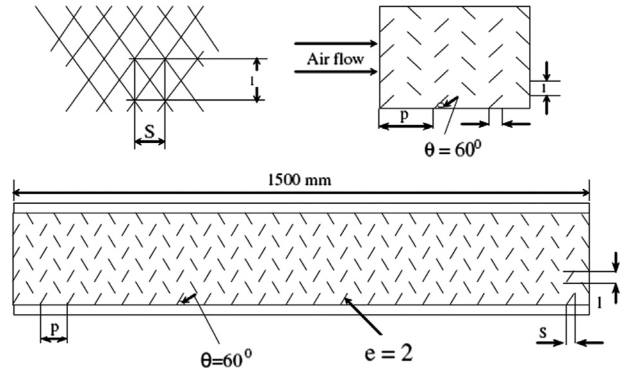


Fig. 35. Metal grit ribs.

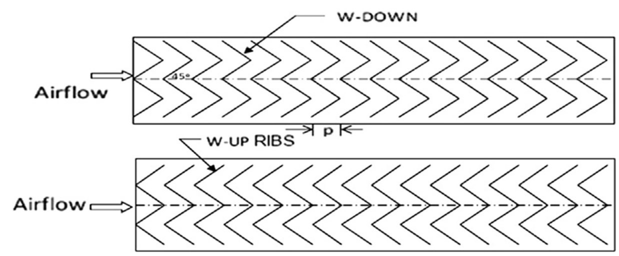


Fig. 36. W-shaped rib.

5.13. Metal grit ribs

Karmare et al. [46] experimentally study the effect of heat transfer performance of a rectangular duct with metal grit ribs as roughness element as shown in Fig. 35, employed on one broad wall, transferring heat to the air flowing through it. The effect of relative length, height and pitch of metal grid ribs on the heat transfer and friction factor has been studied for the flow range of Reynolds numbers 4000–17,000. It has been found that maximum heat transfer rate was reported for the set of parameters ($l/s=1.72$, $e/D_h=0.044$, $P/e=17.5$) and maximum friction factor was observed for the set of parameters ($l/s=1.72$, $e/D_h=0.044$, $P/e=12.5$). Correlation for Nusselt number and friction factor were developed based on the experimental results.

5.14. W-shaped ribs

The experimental investigation of heat transfer and friction factor characteristics of a rectangular duct roughened with W-shaped ribs arranged at an inclination with respect to the flow direction on its underside on one broad wall was conducted by Lanjewar et al. [47]. The duct had a width to height ratio (W/H) of 8.0, relative roughness pitch (P/e) of 10, relative roughness height (e/D_h) of 0.03375 and angle of attack of flow (α) of 30°–75°. W ribs had been tested both pointing in downstream W-down and upstream W-up to the flow. W-down ribs provide better thermo-hydraulic performance than W-up and V-ribs. Highest enhancement in thermo-hydraulic performance for W-down ribs was 1.98 while it was 1.81 for W-up ribs in the range of parameters investigated. The geometry has been shown in Fig. 36.

5.15. Discrete W-shaped ribs

Kumar et al. [48] experimentally investigated heat transfer and friction characteristics in a solar air heater having absorber plate

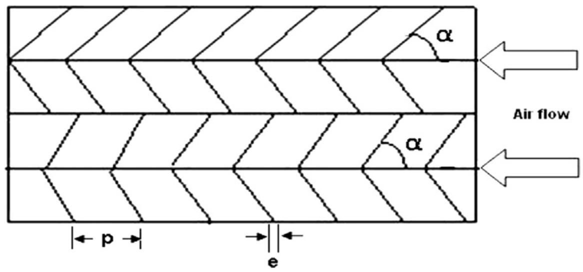


Fig. 37. Discrete W shaped ribs.

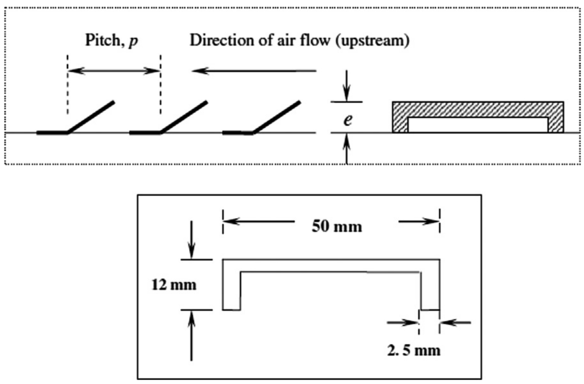


Fig. 38. U-shaped tabulators.

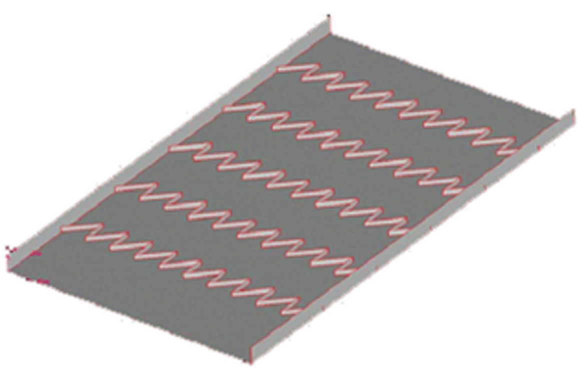


Fig. 39. Z-shaped rib.

roughened with discrete W-shaped ribs. It was investigated that, thermal performance of the roughened channel was 1.2–1.8 times the smooth channel for range of parameters investigated. The maximum enhancement of Nusselt number and friction factor was reported as 2.16 times and 2.75 times that of smooth duct, analogous to angle of attack of 60° and relative roughness height of 0.0338. The geometry investigated has been shown in Fig. 37.

5.16. U-shaped ribs

An experimental investigation had been carried out by Bopche et al. [49] to study the heat transfer coefficient and friction factor by using artificial roughness in the form of inverted U-shaped turbulators as shown in Fig. 38, on the absorber surface of an air heater duct. As compared to the smooth duct, the enhancement in heat transfer and friction factor was reported of the order of 2.82 and 3.72 times, respectively. At Reynolds number, Re=3800, the maximum enhancement in Nusselt number and friction factor are of the order of 2.388 and 2.50, respectively. Better thermo hydraulic performance was reported due to generation of turbulence only in the viscous sub layer region.

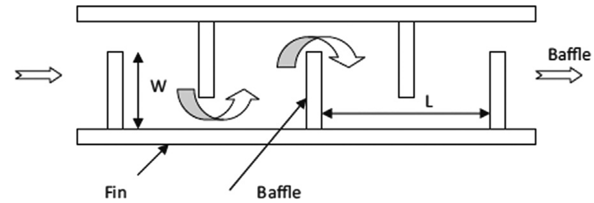


Fig. 40. Baffle arrangement on absorber plate.

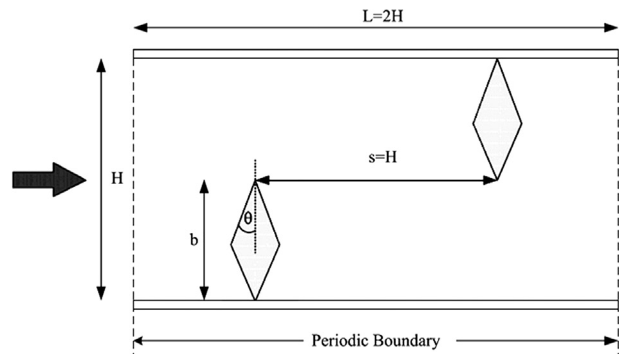


Fig. 41. Staggered diamond shape baffle.

5.17. Z-shaped ribs

Sriromrein et al. [50] studied heat transfer and friction characteristic of a rectangular duct roughened artificially with Z-shape ribs as shown in Fig. 39. The enhancement in heat transfer rate and best thermal performance was reported for Z-rib inclined at 45°.

5.18. Solid baffles

The efficiency of solar air heaters with baffles as shown in Fig. 40 was experimentally investigated by Yeh et al. [51]. Solar air heaters with fins in the collector were provided with attached baffles which creates air turbulence and an extended heat transfer area. This arrangement caused a considerable improvement in collector efficiency. It was studied that increasing the density of baffles also increases the collector efficiency but this will increase the power consumption by blower.

Theoretical investigation of the effect of collector aspect ratio on collector efficiency of baffled solar air heaters was carried out by Yeh et al. [52]. They investigated that with increase in aspect ratio, the collector efficiency is also increases. Numerical investigation of laminar periodic fluid flow and heat transfer in the entrance region of a two dimensional horizontal channel with isothermal walls and with staggered baffles was conducted by Sripattanapipat et al. [53] as shown in Fig. 41. Effects of different baffle tip angles on heat transfer and pressure loss in the channel were studied and the results of the diamond baffle were compared with those of the flat baffle. The order of enhancement was reported about 200–680% for using the diamond baffles. However, as predicted, the augmentation was associated with enlarged friction loss ranging from 20 to 220 times above the smooth channel.

Numerical simulations of three-dimensional laminar forced convection flow adjacent to backward-facing step in rectangular duct were presented by Nie et al. [54] to inspect effects of the baffle on flow and heat transfer distributions. Investigators maintained step height as constant and baffle were mounted onto the upper wall and its distance from the backward-facing step is varied. They reported that this arrangement of baffles increases

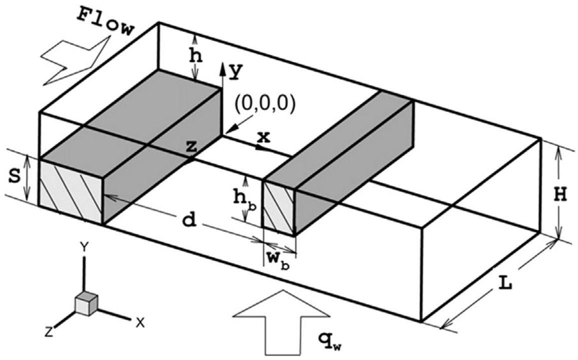


Fig. 42. Schematic of computational domain.

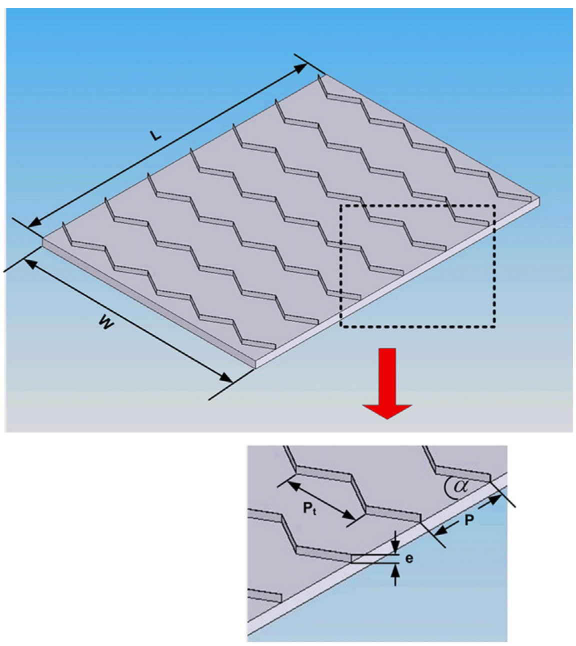


Fig. 43. Multiple 60° V-baffles.

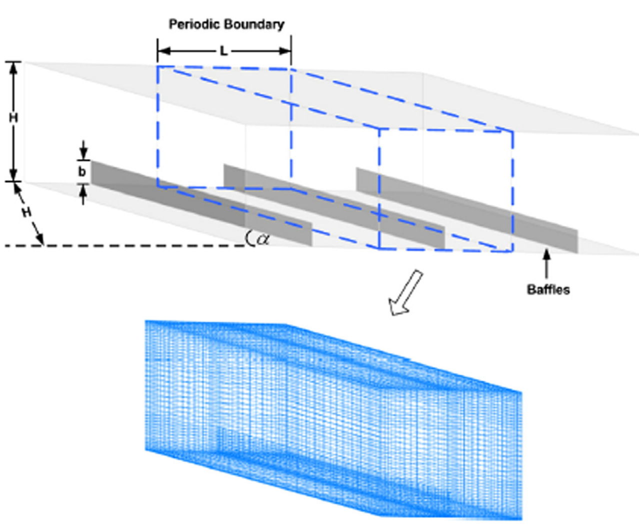


Fig. 44. Computational domain of periodic flow.

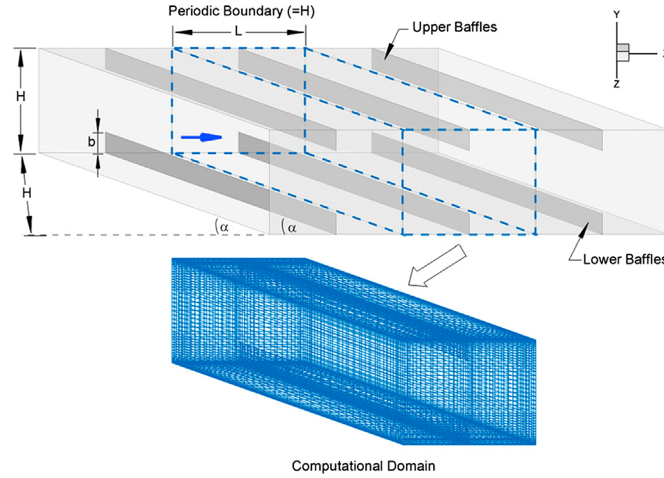


Fig. 45. Duct geometry and computational domain with baffles.

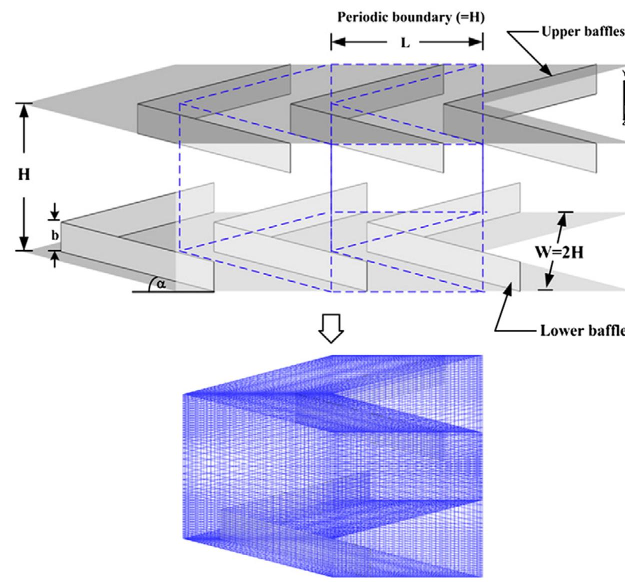


Fig. 46. Duct geometry and computational domain.

the magnitude of maximum Nusselt number at the stepped wall. The maximum Nusselt number on the stepped wall was developed near the sidewall, and it moved further downstream as the location of the baffle moves in the streamwise direction. The friction coefficient at the stepped wall decreases as the distance of the baffle from the inlet increases. Schematic of computational domain is shown in Fig. 42.

Promvonge [55] carried out an experimental investigation to assess turbulent forced convection heat transfer and friction loss behaviors for airflow through a channel fitted with a multiple 60° V-baffle turbulator as shown in Fig. 43. Experiment was carried out using a channel of aspect ratio, AR=10 and height, H=30 mm with three different baffle blockage ratios, (e/H=0.10, 0.20 and 0.30) and three baffle pitch spacing ratios, (PR=P/H=1, 2 and 3) while the transverse pitch of the V-baffle is set to 2H and kept constant.

The experimental results confirmed that the V-baffle provides the drastic increase in Nusselt number, friction factor and thermal enhancement factor values over the smooth wall channel due to better flow mixing from the formation of secondary flows induced by vortex flows generated by the V-baffle. Significant increase in Nusselt number and friction factor values were found for the rise in blockage ratio and/or for the decrease in pitch ratio values. At lower Reynolds number, the use of V-baffle with e/H=0.10 and PR=1, reported the highest value of 1.87 for thermal enhancement factor.

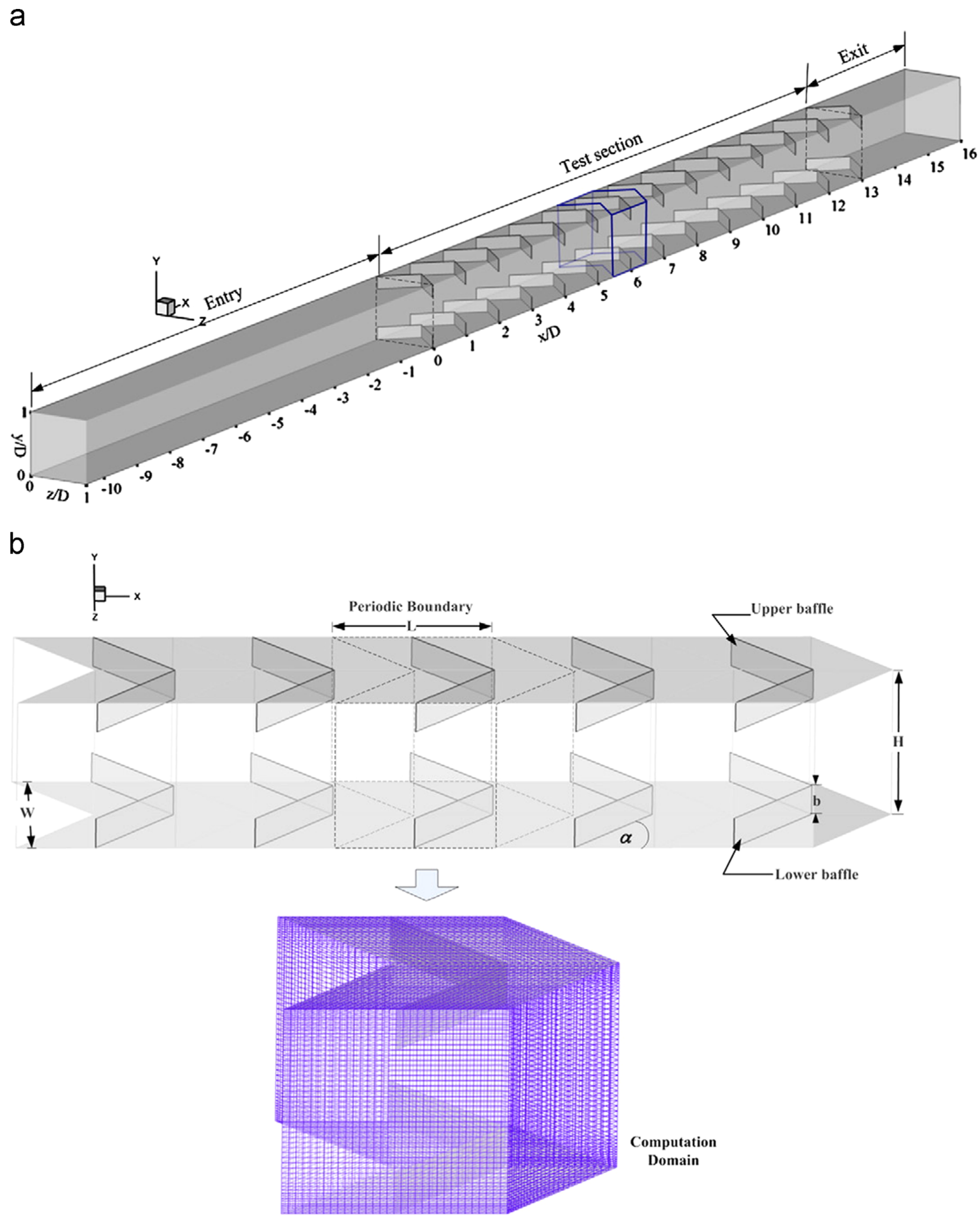


Fig. 47. Computational domain with baffles.

Promvonge et al. [56] carried out a numerical investigation on periodic laminar flow and heat transfer behaviors in a three-dimensional isothermal wall square-channel fitted with 30° angled baffles on two opposite channel walls as shown in Fig. 44. The angled baffles with the attack angle of 30° were mounted periodically and inline arrangement on the lower and upper channel walls. This arrangement caused a pair of stream wise counter-rotating vortex (P-vortex) through the channel. They studied the effects of different baffle heights and three pitch ratios on heat transfer and flow behaviors in the channel.

Heat transfer enhancement was reported as 1.2–11 times for using the 30° baffle pair with BR=0.1–0.3 and PR=1, 1.5 and 2. Penalty of pressure loss in the range 2 to 54 times above the smooth channel was also reported by investigators. The maximum value of thermal enhancement factor was found to be 4.0 at highest Reynolds number and PR=2. When effect of the baffle PR and BR values on heat transfer rate is examined, it was found that the maximum enhancement factor is about 4.0 for BR=0.15, PR=2.0 and Re=2000.

Promvonge et al [57] carried out numerical study on periodic laminar flow and heat transfer behaviors in a three dimensional isothermal wall square channel fitted with 30° angled baffles on one channel wall as shown in Fig. 45. The range of parameters used for the experiment were Reynolds number in the range of 100–2000, PR=1,1.5 and 2, BR=0.1–0.5. In this study, heat transfer enhancement was reported as 1.00–9.23 times for using baffle with BR=0.1–0.5. The pressure loss penalty was reported in the range of 1.09 to 45.31 times over the smooth duct. Maximum value of thermal enhancement factor was found to be 3.1 at BR=0.3 and PR=1.5.

A numerical investigation had been carried out by Promvonge et al. [58] to examine periodic laminar flow and heat transfer characteristics in a three-dimensional isothermal wall channel of aspect ratio, AR=2 with 45° staggered V-baffles as shown in

Fig. 46. V-baffles with an attack angle of 45° were mounted in tandem and staggered arrangement on the lower and upper walls of the channel to generate two pair of main stream wise vortex flows through the tested section. Heat transfer enhancement was about 100–1100% for using both the 45° baffles with BR=0.05–0.3 and pressure loss ranging from 2 to 90 times above the smooth channel. Maximum value of thermal enhancement factor was reported as about 2.6–2.75 indicating higher thermal performance over smooth channel.

A numerical investigation on laminar flow and heat transfer characteristics in a three dimensional isothermal wall square-channel fitted with inline 45° V-shaped baffles on two opposite wall was done by Promvonge et al. [59]. The inline V-baffles with its V-tip pointing downstream and the attack angle (or half V-apex angle) of 45° relative to the flow direction were mounted repeatedly on the lower and upper walls. The V-baffled channel flow was found to be fully developed periodic flow and heat transfer profiles at about $x/D \approx 8$ downstream of the tested channel inlet. It was reported that the P-vortex flow caused by the V-baffle induced impingement/attachment flows on the channel walls leading to drastic increase in the heat transfer rate. The heat transfer in the V-baffled channel was found to be about 1–21 times higher than the smooth channel with no baffle. However, this also results in friction loss ranging from about 1.1 to 225 times above the smooth channel. The computational domain is shown in Fig. 47.

A numerical investigation had been carried out by Promvonge et al. [60] to examine laminar flow and heat transfer characteristics in a three-dimensional isothermal wall square channel with 45°-angled baffles as shown in Fig. 48. In order to generate a pair of mainstream wise vortex flows through the tested section, baffles with an attack angle of 45° were mounted in tandem and inline arrangement on the lower and upper walls of the channel. Effects of different baffle heights on heat transfer and pressure loss in the channel were studied and the results of the 45° inline baffle were also compared with those of the 90° transverse baffle and the 45° staggered baffle. The presence of 45° baffles creates P-vortex flow which helps to induce impingement flows on the BLE sidewall and wall in the baffle cavity leading to drastic increase in heat transfer in the square channel. The enhancement was in the order of 150–850% for using both the 45° baffles with BR=0.05–0.3. On the other hand, the heat transfer augmentation is associated with enlarged pressure loss ranging from 2 to 70 times above the

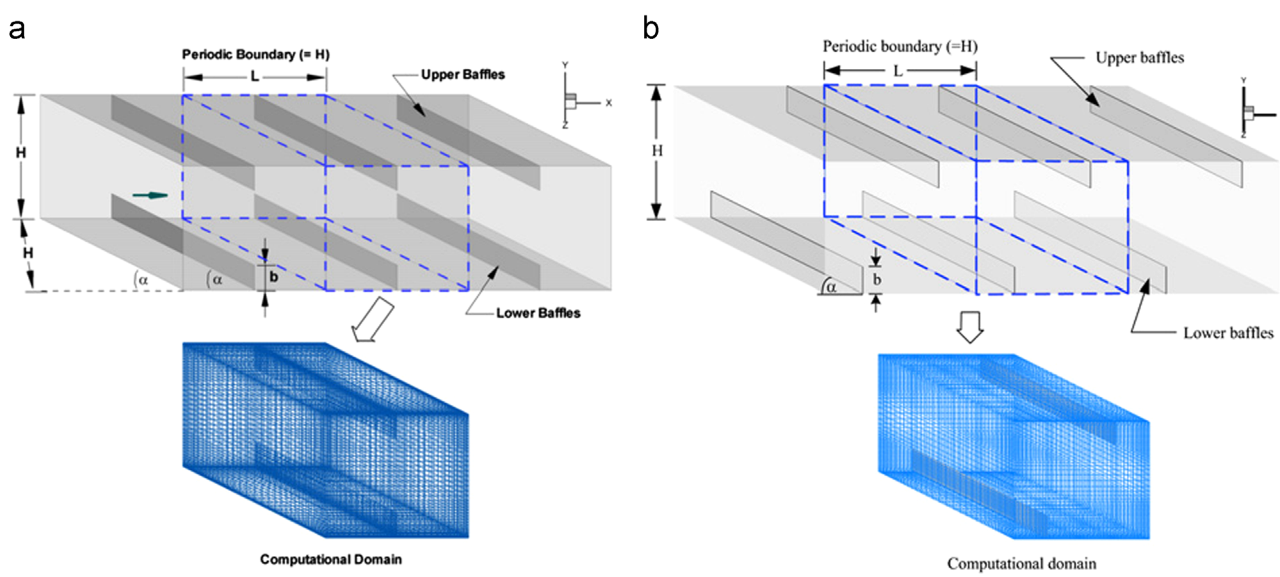


Fig. 48. (a) Inline and (b) staggered arrangement of baffles.

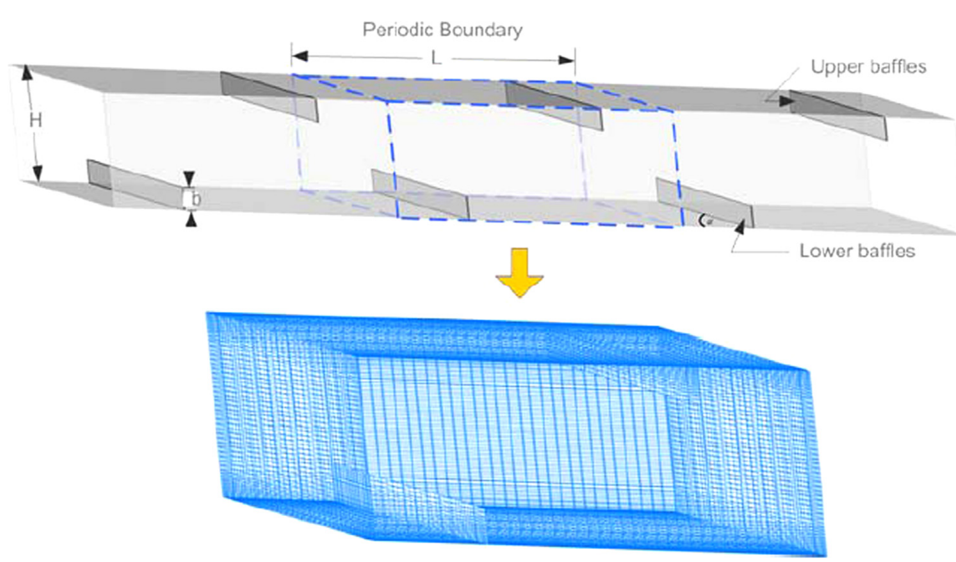


Fig. 49. Channel geometry and computational domain with baffles.

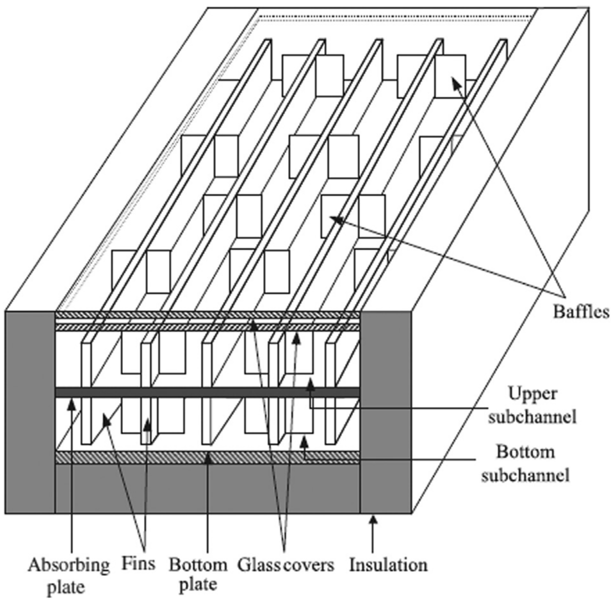


Fig. 50. Double pass solar air heater with fins and baffles.

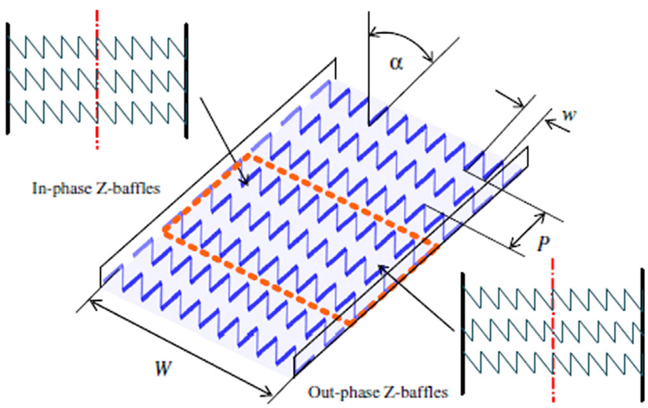


Fig. 51. Arrangement of Z shaped baffles in a test section.

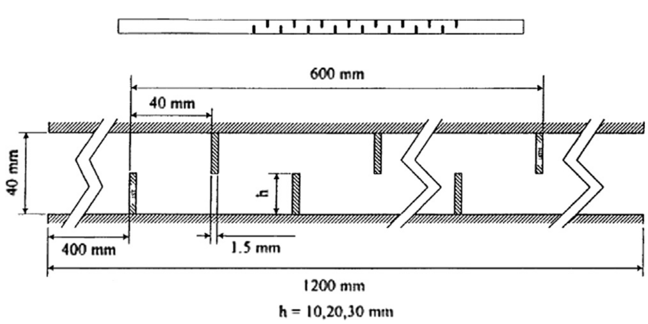


Fig. 52. Channel with porous baffles.

smooth channel. They investigated that for the 45° baffles, the heat transfer enhancement was around 100–200% higher than that for the 90° baffle whereas the friction loss can be reduced at about 10–150%.

A numerical investigation had been carried out by Kwankaomeng et al. [61] to study laminar flow and heat transfer characteristics in a three-dimensional isothermal wall square-channel with 30° staggered angled-baffles. They studied the effects of different baffle heights at a single pitch ratio (PR=3) on heat transfer and pressure loss in the channel. The vortex flows was created by using the 30° angled baffles help to induce impingement flows on the sidewall and the wall in the inter baffle cavity leading to drastic

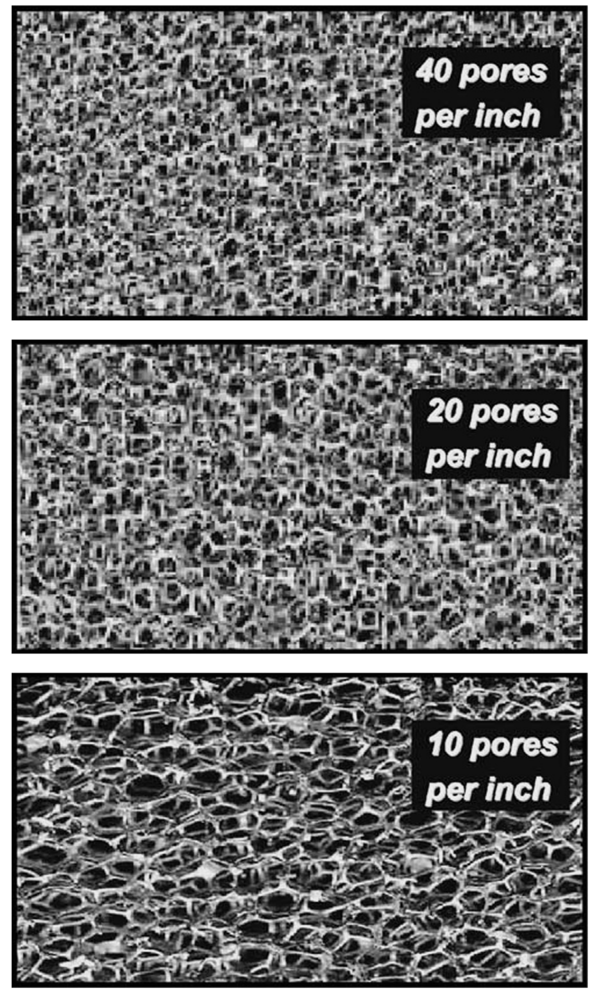


Fig. 53. Aluminum foam structure.

increase in heat transfer in the channel. The order of enhancement is about 100–650% for using the angled baffles with BR=0.1–0.3. The heat transfer augmentation was associated with enlarged pressure loss ranging from 1 to 17 times above the smooth channel. Thermal enhancement factors for the inclined baffles at BR=0.15 was found to be highest about 2.9. The channel geometry with computational domain is shown in Fig. 49.

The performance of a solar air heater featured with double-pass as well as fins and baffles design was investigated by Chii-Dong et al. [62] using both experimental and theoretical approaches, for the effect of recycling operation. The performances of the new design and the other two designs, which are double-pass without fins and double-pass with fins only, were compared. The best collector efficiency was reported for new design as compared to all other designs under recycling operation. But mainly, the improvement of collector efficiency was found due to use of baffles. The best possible reflux ratio for the fined plus baffled double-pass design was investigated about 0.5 while considering both the collector efficiency and the pumping power requirement. A schematic drawing of a fined plus baffled double pass solar air heater is shown in Fig. 50.

The influence of baffle turbulators on heat transfer augmentation in a rectangular channel of aspect ratio of 10 fitted with the in-phase and out-phase 45° Z-baffles in the turbulent regime from Re=4400 to 20,400 had been investigated experimentally and numerically by Sriromreun et al. [63]. In the experiment, the baffles were placed in a zigzag shape (Z-shaped baffle) aligned in series on the isothermal-fluxed top wall, similar to the absorber

plate of a solar air heater channel. The intension of using the Z-baffles was to create co-rotating vortex flows having a significant influence on the flow turbulence intensity leading to higher heat transfer enhancement in the tested channel. Effects of the Z-baffle height and pitch spacing length were examined to find the optimum thermal performance for the Reynolds number from 4400 to 20,400. The Z-baffles inclined to 45° relative to the main flow direction were characterized at three baffle to channel-height ratios (e/H=0.1, 0.2 and 0.3) and baffle pitch ratios (P/H=1.5, 2 and 3).

For the in-phase baffle array at P/H=1.5, the increases in Nu with the e/H=0.1, 0.2 and 0.3 were in the range of 430–440%, 530–550% and 640–670% over the smooth channel, respectively. Moreover, the use of Z-baffles with e/H=0.3 were reported to give higher heat transfer than that with e/H=0.2 and 0.1 around 10% and 30%, respectively. The friction factor value of the Z-baffle at P/H=1.5 and e/H=0.3 was found to be around 2 and 5 times higher than that with e/H=0.2 and 0.1, respectively.

For the in phase Z-baffle at e/H=0.1, the increases of the Nu for P/H=1.5, 2 and 3 were in a range of 430–440%, 310–380% and 310–330% over the smooth channel, respectively. Importantly, the Z-baffle with e/H=0.1 at P/H=1.5 shows higher heat transfer rate than the one at P/H=2 and 3 around 15% and 30%, respectively.

The arrangement of baffles is shown in Fig. 51.

5.19. Porous and perforated baffles

Numerical predictions on the turbulent fluid flow and heat transfer characteristics for rectangular channel with porous baffles which are arranged on the bottom and top channel walls in a periodically staggered way was studied by Yang and Hwang [64]. The Experimental parameters studied include the entrance Reynolds number Re (1×10^4–5×10^4), the baffle height (h/H=0.25, 0.5 and 0.75 mm), porosities (υ=0.2, 0.42 and 0.7) and kind of baffles (solid and porous); whereas the baffle spacing S/H are fixed at 1.0 and the working medium used by them was air. They found that if the solid baffles were replaced by porous type baffles, there was reduction in effective thermal conductivity of the baffle, heat transfer surface was increased and the flow transport phenomenon was changed. Friction factor had a lower value for the porous-type baffle channel relative to the solid-type baffle channel because of less channel blockage. A schematic diagram of forced convection enhancement in a channel using porous baffles is shown in Fig. 52.

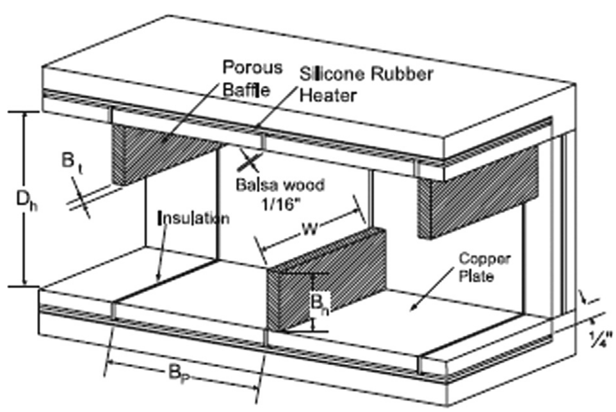


Fig. 54. Schematic of test section.

Ko and Anand [65] carried out experimental investigation to measure module average heat transfer coefficients in uniformly heated rectangular channel with wall mounted porous baffles. They mounted baffles on top and bottom of the walls alternatively. Investigation reported that the heat transfer enhancement ratio decreases with increase in Reynolds number and increases with increase in pore density. The heat transfer enhancement ratio was found to be higher for taller (B_h/D_h=2/3) and thicker (B_t/D_h=1/3) baffles. The friction factor slightly decreased with increase in Reynolds number, and increased with baffle thickness and pore density. Material used for the baffles are shown in Fig. 53. Details of the test section are shown in Fig. 54.

Experimental investigations were carried out by Tzeng [66] to determine the local and average heat transfer characteristics in asymmetrically heated sintered porous channels with metallic baffles. The solid baffles were inserted periodically into the sintered metallic materials in four modes as shown in Fig. 55. They also examined the effect of the bead diameter of sintered metallic materials. The heat transfer by convection in all modes was increased as the bead diameter declined. It was studied that at Re > 2000, heat transfer enhancement was found to be more in mode B and worst in mode D even less than that in mode A. At a Re of about 1000, there was heat transfer enhancement in mode D.

5.20. Perforated baffles

Lin [67] analyzed the experimental results of heat transfer for baffles designed with different heights (H=10–50 mm) and pores (N=1–3) in the event of five Reynolds numbers (702–1052) and three heating quantities (q_{in}=90–750 W/m^2) as well as heat flux (Q=40–100 l/min). It was studied that maximum Nusselt number

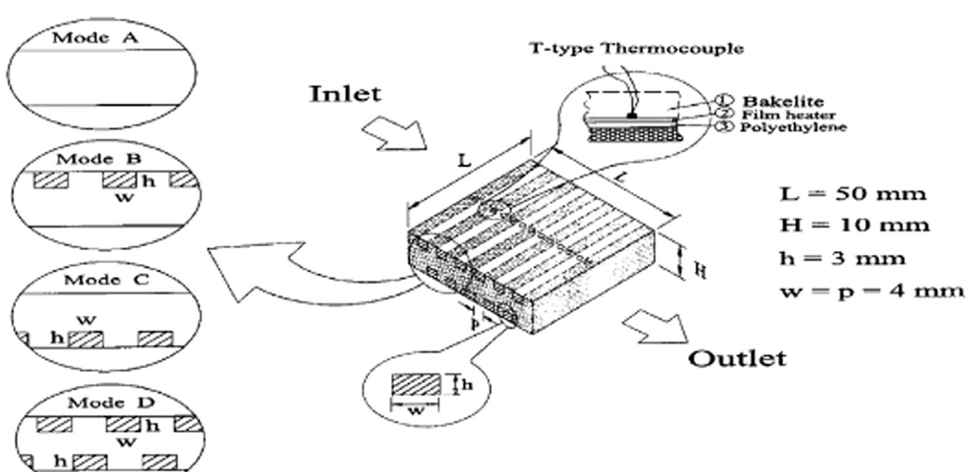


Fig. 55. Modes of test specimens and measured positions of thermocouples.

without baffles of pores was generated at $q_{in}=750\ W/m^2$, Re = 1752 at $X/L=0.04$. It was found that the distribution of Nusselt number declines gradually with the increase of X/L, and its minimum value was generated at $X/L=0.68$, with a nearly one time difference with the maximum value. The biggest difference occurred at $X/L=0.2$, with the difference of Nusselt number approx. 50%. In the case of $X/L>0.68$, Nusselt number gradually increases, so Nusselt number at rear section is higher than that at middle section, i.e. outlet effect.

Experimental study was performed by Huang et al. [68] for a measurement of heat transfer coefficients in a square channel with a perforation baffle by using the transient liquid crystal technique, and also studied the effects of Reynolds number and the height of the perforation baffle on Nusselt numbers. Local heat transfer enhancement at the downstream of step baffle was found to be more significant when Reynolds number was large and when baffle height was higher. Heat transfer coefficient off center was found to be better because of secondary flows that appeared off center after the airflow passes through the baffle. The heat transfer enhancement in case of a baffle with holes was reported greater than that without holes.

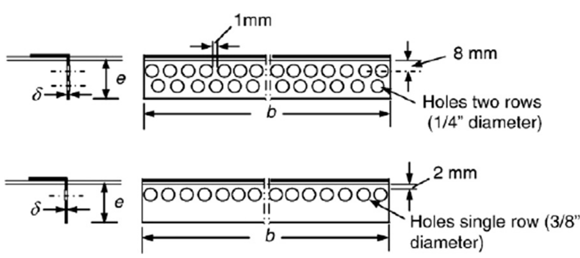


Fig. 56. Fully perforated baffles and half perforated baffles with two and single rows of holes respectively.

Karwa and Maheshwari [69] made an experimental study of heat transfer and friction in a rectangular section duct with fully perforated baffles (open area ratio of 46.8%) or half perforated baffles (open area ratio of 26%) at relative roughness pitch of 7.2–28.8 affixed to one of the broader walls as shown in Fig. 56. They investigated that there was an enhancement of 79–169% in Nusselt number over the smooth duct for the fully perforated baffles and 133–274% for the half perforated baffles while the friction factor for the fully perforated baffles was found to be 2.98–8.02 times of that for the smooth duct and 4.42–17.5 times for the half perforated baffles.

5.21. Delta winglet

In order to enhance the rate of heat transfer in engineering devices like heat exchanger, vortex combustor, drying process etc, secondary or rotary flow is created using swirl or vortex generators that are inserted in main flow. These are made in triangular or rectangular shapes and can be welded or punched and bend out of the plate so that they project into the flow with an angle of attack to the main flow direction as shown in Fig. 57. Using delta wing vortex generator, enhancement in average heat transfer at low Reynolds number was found to be about 50%–60% [70].

An experimental study was carried out by Torii et al. [71] to obtain heat transfer and pressure loss in a test section, simulated to a fin-and-tube heat exchanger, with in-line or staggered tube banks with delta winglet vortex generators of various configurations as shown in Fig. 58. The proposed "common flow up" configuration causes significant separation delay, reduces form drag, and removes the zone of poor heat transfer from the near-wake of the

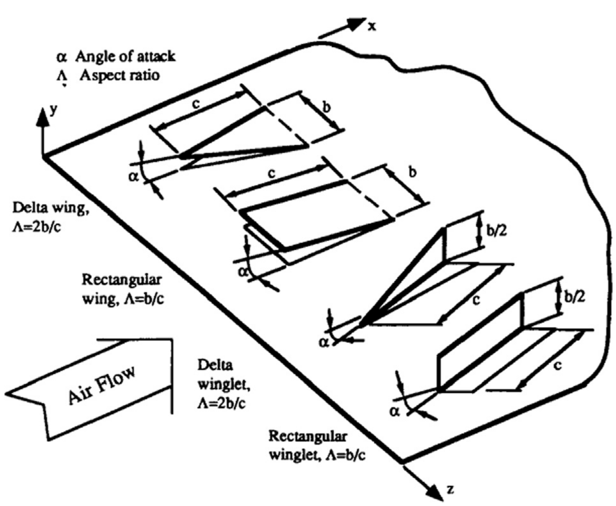


Fig. 57. Different types of longitudinal vortex generators.

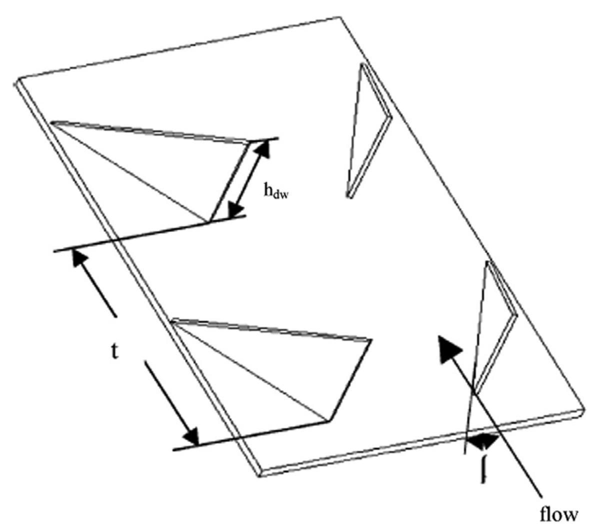


Fig. 59. Schematic of delta winglet.

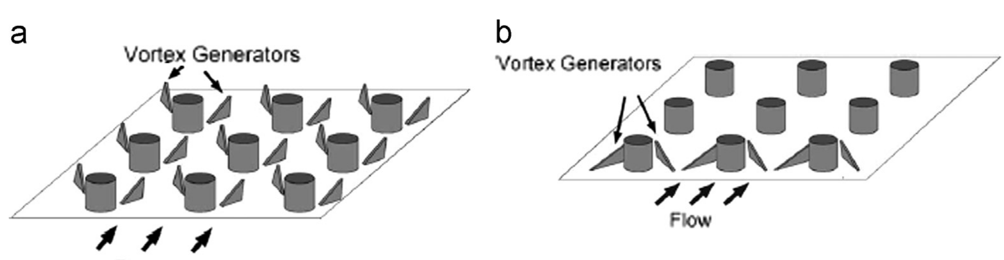


Fig. 58. Configuration of winglet type vortex generator on the fin surface-tube bank: (a) "common flow down" configuration; (b) "common flow up" configuration.

tubes. In case of staggered tube banks, the heat transfer was augmented by 30% to 10%, and yet the pressure loss was reduced by 55% to 34% for the Reynolds number (based on two times channel height) ranging from 350 to 2100, when the present winglets were added. In case of in-line tube banks, these were found to be 20% to 10% augmentation, and 15% to 8% reduction, respectively.

An experimental study was carried out by Yakut et al. [72] to study the effects of various kinds of design parameters on the heat transfer and flow characteristics of the tapes with delta-winglet vortex generators were systematically analyzed using the Taguchi method. The maximum heat-transfer rate was observed at 16,906 Reynolds number, 60° angle of attack, 16 mm winglet height and 25 mm pitch of the winglets and the minimum friction factor was observed at 8 mm winglet height, 16906 Reynolds number, 30° angle of attack and 75 mm pitch. The maximum vortex-shedding frequency occurred at 16,906 Reynolds number, 25 mm pitch, 8 mm winglet height and 30° angle of attack. The minimum vortex-shedding frequency was obtained at 3690 Reynolds number, 75 mm pitch, 16 mm winglet height and 90° angle of attack.

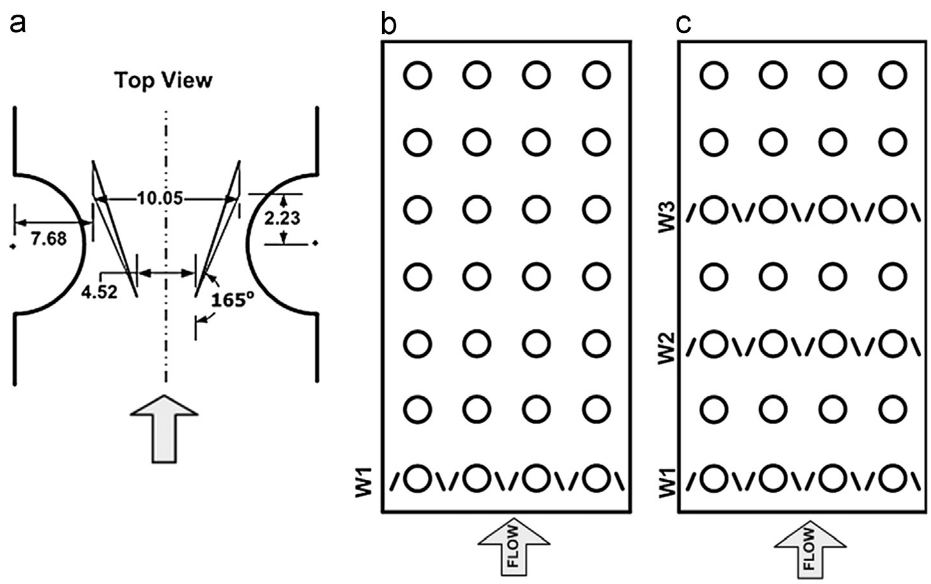


Fig. 60. (a) Winglet vortex generator dimensions; (b) single row; (c) three row inline array configurations.

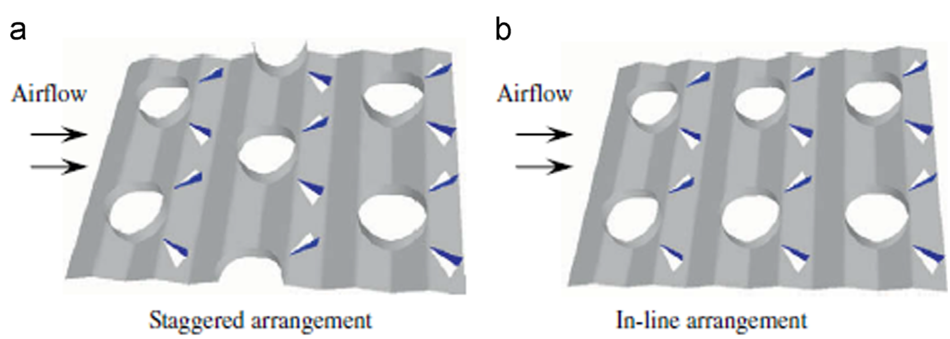


Fig. 61. Schematic of delta winglets in (a) staggered and (b) inline arrangement.

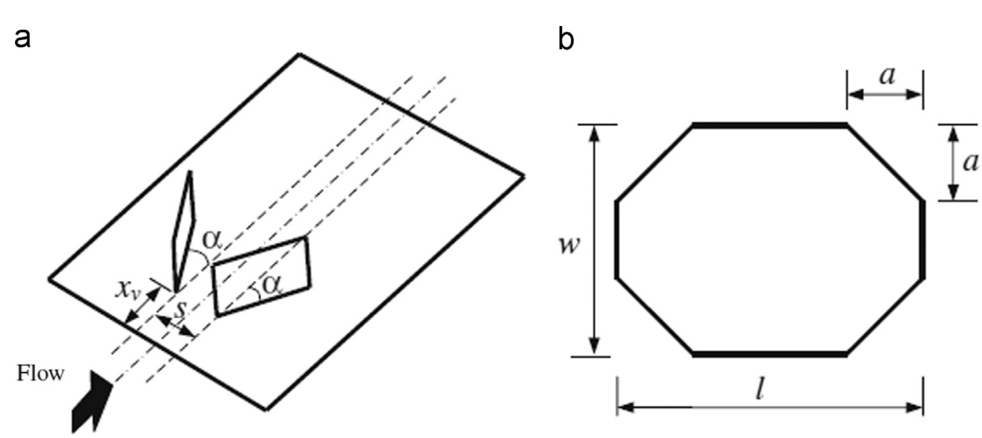


Fig. 62. Schematic view of present modified longitudinal vortex generator: (a) layout of common-flow-down wings; and (b) modified rectangular wing.

The optimum results were obtained at 25 mm pitch, 8 mm height of winglet, 30° angle of attack and a Reynolds number of 16,906 for larger frequencies required to avoid resonance. For smaller frequencies, in order to avoid resonance, the optimum results were 75 mm pitch, 8 mm height of winglet, 60° angle of attack and a Reynolds number of 16,906. Geometry used for the investigation is shown in Fig. 59.

The potential of winglet type vortex generator (VG) arrays for air-side heat transfer enhancement was experimentally evaluated by full-scale wind-tunnel testing of a compact plain-fin-and-tube heat exchanger by Joardar et al. [73] as shown in Fig. 60. They

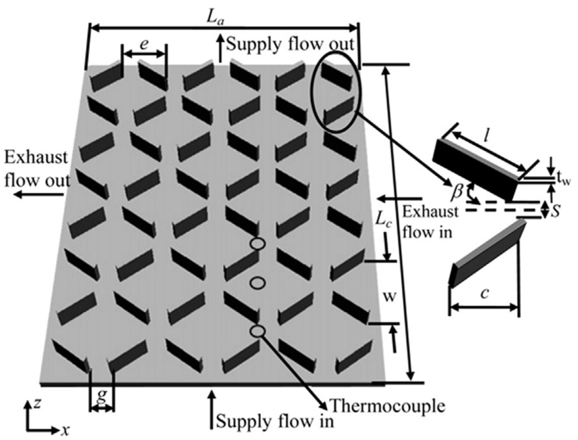


Fig. 63. Placement of winglets in rectangular channel.

studied that the air-side heat transfer coefficient increases from 16.5% to 44% for the single-row winglet arrangement with an increase in pressure drop of less than 12%. For the three-row vortex generator array, the enhancement in heat transfer coefficient increases with Reynolds number from 29.9% to 68.8% with a pressure drop penalty from 26% at Re = 960 to 87.5% at Re = 220.

Tian et al. [74] carried out a three-dimensional numerical simulation to study the air-side performance of a wavy fin-and-tube heat exchanger with delta winglets in terms of heat transfer and fluid flow characteristics. The wavy fin-and-tube heat exchangers which have three-row round tubes in staggered or inline arrangements were studied. They studied that when , $Re_{Dc} = 3000$, compared with the wavy fin, the *j* and *f* factors of the wavy fin with delta winglets in staggered and in-line arrays are increased by 13.1%, 7.0% and 15.4%, 10.5%, respectively. Geometry investigated is shown in Fig. 61.

Fluid flow and heat transfer characteristics of a modified rectangular longitudinal vortex generator (LVG) as shown in Fig. 62, obtained by cutting off the four corners of a rectangular wing was studied by Min et al. [75] experimentally. Study shows that the modified rectangular wing pairs (MRWPs) have better flow and heat transfer characteristics than those of rectangular wing pair (RWP). It was found that at $z = \pm 40$ mm from the centerline of the heater plate, the local heat transfer is enhanced due to the strong longitudinal vortices generated by the presence of the LVGs.

Second law analysis of a cross-flow heat exchanger (HX) was done by Kotcioglu et al. [76]. The entropy generation in a cross-flow HX with a new winglet-type convergent-divergent

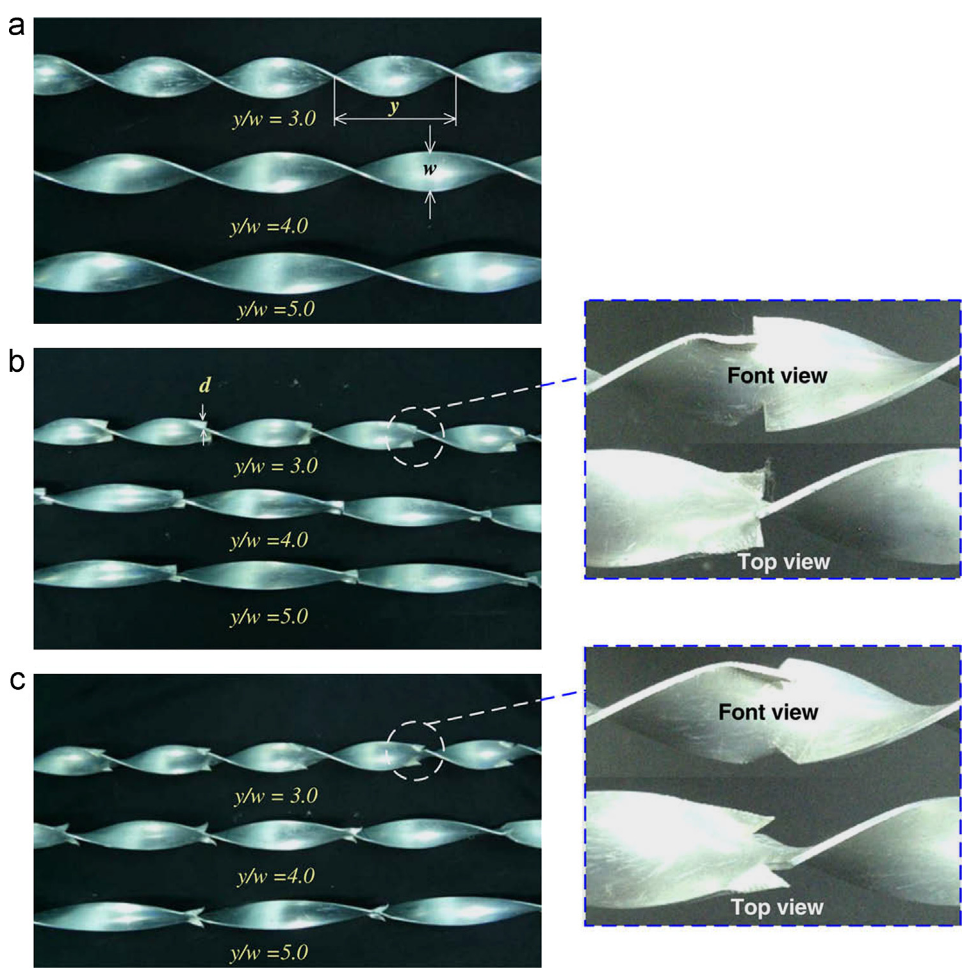


Fig. 64. Twisted tape vortex generator: (a) typical twisted tape (TT), (b) straight delta-winglet twisted tapes (S-DWT) and (c) oblique delta-winglet twisted tapes (O-DWT).

longitudinal vortex generator (CDLVG) is investigated and is shown in Fig. 63. They found that at the low Reynolds number, the entropy generation number was influenced by the heat transfer while at the high Reynolds number, it was influenced by the pressure drop. Another conclusion reported that, the present vortex generator (CDLVG) shows an increase in the heat transfer enhancement from 15% to 30% and also an increase in the pressure-loss penalty from 20% to 30%, in a comparison with and without vortex generators, respectively.

Experimental investigations of heat transfer, flow friction and thermal performance factor characteristics in a tube fitted with delta winglet twisted tape, using water as working fluid was done by Eiamsa-ard et al. [77]. In the study, they described the influences of the oblique delta-winglet twisted tape (O-DWT) and straight delta-winglet twisted tape (S-DWT) arrangements. They reported that the O-DWT is more effective turbulator giving higher heat transfer coefficient than the S-DWT. Over the range considered, Nusselt number, friction factor and thermal performance factor in a tube with the O-DWT are, respectively, 1.04–1.64, 1.09–1.95, and 1.05–1.13 times of those in the tube with typical twisted tape (TT). Geometry investigated is shown in Fig. 64.

Champookham et al. [78] carried out experimental investigations to study the effect of combined wedge ribs and winglet type vortex generators (WVGs) on heat transfer and friction loss behaviors for turbulent airflow through a constant heat flux channel. Two types of wedge rib viz. wedge ribs pointing downstream and pointing upstream were arranged in the form of inline and staggered style. Two pairs of the WVGs with the attack angle of 60° were mounted on the test channel entrance so as to generate longitudinal vortex flows through the tested section. The test channel had an aspect ratio, AR=10 and height, $H=30$ mm with a rib height, $e/H=0.2$ and rib pitch, $P/H=1.33$ with the Reynolds number range of 5000–22,000. Investigations

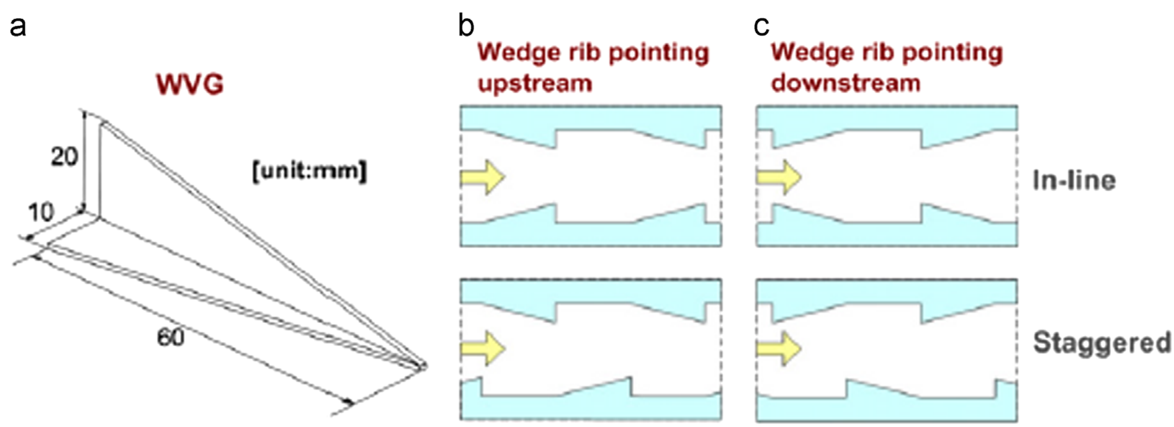


Fig. 65. (a) winglet geometry, (b) wedge rib pointing upstream and (c) wedge rib pointing downstream.

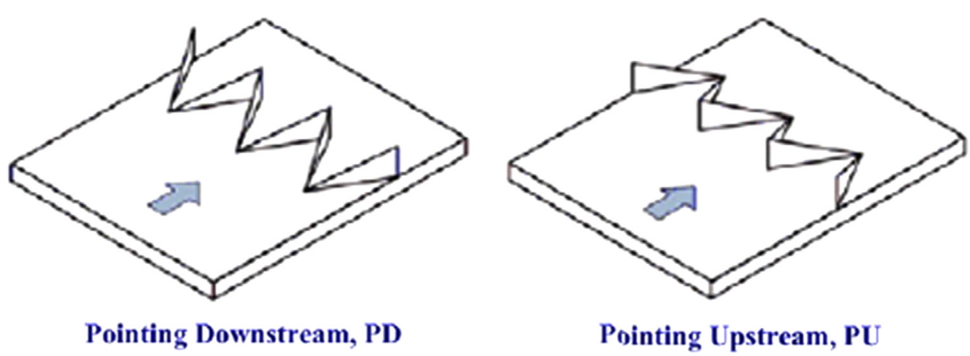


Fig. 66. Delta winglets pointing downstream (PD) and pointing upstream arrangement.

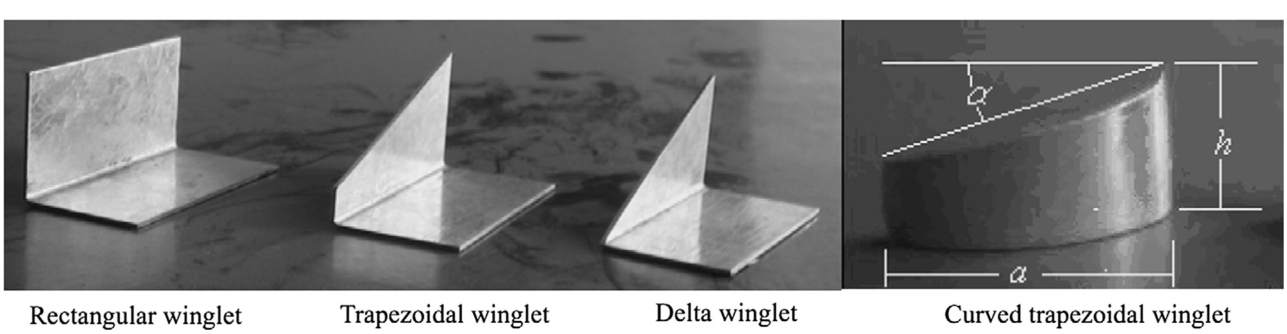


Fig. 67. Different types of vortex generators under study.

reported that the use of the wedge rib turbulators with $e/H = 0.2$ causes a high pressure drop increase, specially for the in-line wedge pointing downstream and also provides considerable heat transfer augmentations, $Nu/Nu_0 = 2.9–3.5$ for use with the WVGs.

The geometry investigated is shown in Fig. 65.

Promvonge et al. [79] experimentally studied the effects of combined ribs and delta-winglet type vortex generators (DWs) on forced convection heat transfer and friction loss behaviors for turbulent airflow through a solar air heater channel. Rectangular channel with aspect ratio, AR = 10, height, $H = 30$ mm with Reynolds number in the range of 5000–22,000 was used. They reported that combined rib and the DW provides considerable heat transfer augmentations, $Nu/Nu_0 = 2.3–2.6$ and also causes a moderate pressure drop increase, $f/f_0 = 4.7–10.1$, depending on the attack angle and Re values. Another conclusion is that, the use of combined rib and PD-DW at lower angle of attack provides higher heat transfer of about 40–65% and better thermal performance than the rib/the DW alone, leading to more compact heat exchanger. Delta winglet geometries are shown in Fig. 66.

The performance of a pair of new vortex generators called Curved trapezoidal winglet (CTW) had been investigated experimentally by Zhou and Ye [80] and compared with traditional vortex generators – rectangular winglet, trapezoidal winglet and delta winglet as shown in Fig. 67. They studied that Delta Winglet Pair (DWP) is the best in laminar and transitional flow region, while Curved Trapezoidal Winglet Pair (CTWP) has the best thermo hydraulic performance in fully turbulent region due to the streamlined configuration and then the low pressure drop, which indicates the advantages of using this kind of vortex generators for heat transfer enhancement. Small attack angle of CTWP, such as $\beta = 0°$ and 15°, have better thermo hydraulic performance of R than larger attack angles. Particularly, when Re is larger than 18,000, $\beta = 0°$ presents the best thermo hydraulic performance with R as high as 1.6.

5.22. Use of ımpinging jet

Experimental investigation has been carried out by Chauhan et al. [85] to study heat transfer and friction factor characteristics using impinging jets in solar air heater duct. The study shows that there is considerable enhancement in heat transfer and friction factor by 2.67 and 3.5 times respectively. Impingement plate geometry is as shown in Fig. 68.

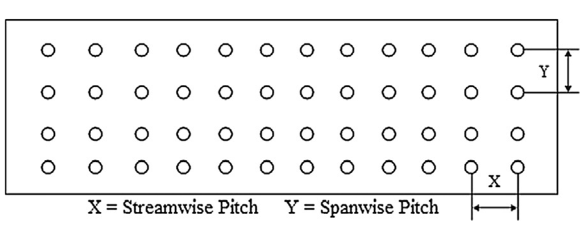


Fig. 68. Impingement plate geometry: location of streamwise and spanwise pitch.

6. Computational analysis

Literature survey in the field of artificially roughened solar air heater reveals that, there are very few attempts had been made in early days because of hardware and development in numerical methodology to solve the complex flow equations. A CFD based investigation of turbulent flow through a solar air heater is carried out by Yadav et al. [86] with square sectioned transverse rib roughness as shown in Fig. 69. The 2D analysis of rectangular duct is performed using ANSYS FlUENT 12.1 software and using RNG k-ε turbulence model. Analysis using four different configurations of rib roughness keeping relative roughness pitch constant at $P/e = 14.29$ and six different values of Reynolds number, ranging from 3800 to 18,000, reveals that the relative roughness height is a vital factor and mainly affects the rate of heat transfer and the increase in flow friction. In this analysis, the maximum value of thermo hydraulic performance parameter (THPP) has been found to be 1.8 for the range of parameters investigated.

Another numerical investigation is conducted by Yadav et al. [87] using FLUENT 12.1 and RNG $k–\varepsilon$ turbulence model on the solar air heater, using square sectioned transverse ribs as shown in Fig. 70, with different values of relative roughness pitch ($7.14 \le P/e \le 17.86$). Reynolds numbers are in the range of 3800 to 18000. This study reported the value of THPP as 1.82 by the use of ribs with P/e of 10.71.

2D CFD analysis to predict the effect of small diameter of transverse wire ribs roughness on heat transfer enhancement in solar air heater is done by Yadav et al. [88]. In this analysis also FLUENT 12.1 software is used with the RNG $k–\varepsilon$ turbulence model. Here the operating parameters are taken as, ($P/e = 7.14–35.71$) and ($e/D = 0.021–0.042$). Here the maximum value of THPP is found to be 1.65 for the range of parameters investigated. The domain used for CFD analysis is shown in Fig. 71.

CFD investigation using ten different ribs namely rectangular, square, chamfered, triangular etc. is done by Chaube et al. [89]. FLUENT CFD code is used for analysis using the SST $k–\varepsilon$ turbulence model. The heat flux of 1100 W/m^2 is provided on the absorber plate only and rib surface is kept adiabatic. Their study reported that highest heat transfer is achieved with chamfered ribs and the best performance index is found with rectangular ribs of size 3 × 5. Two dimensional domain is shown in Fig. 72.

A three dimensional (3D) solar air heater duct provided with artificial roughness in the form of thin circular wire in arc shaped as shown in Fig. 73, has been analyzed by kumar et al. [90] using CFD. Renormalization (RNG) $k–\varepsilon$ turbulence model is used for analysis in FLUENT CFD code. Their study reveals the maximum value of overall enhancement ratio as 1.7 for the range of parameters investigated.

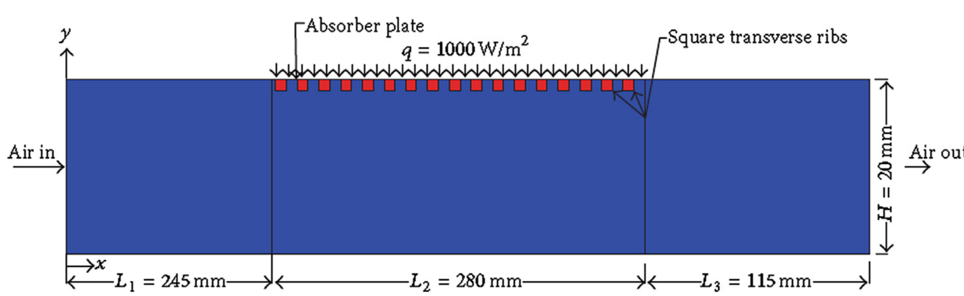


Fig. 69. Geometry of two dimensional domain.

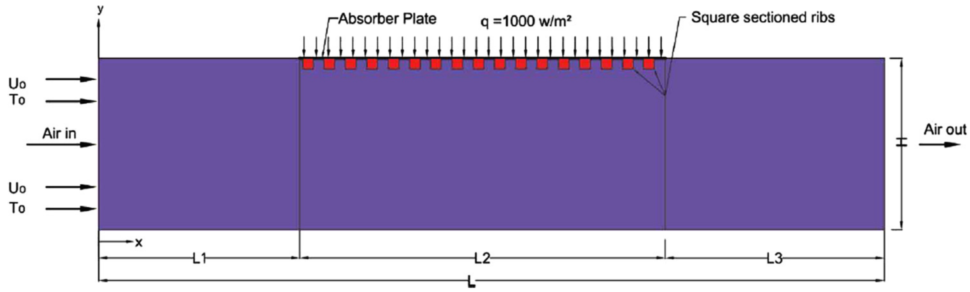


Fig. 70. Schematic of two dimensional domain.

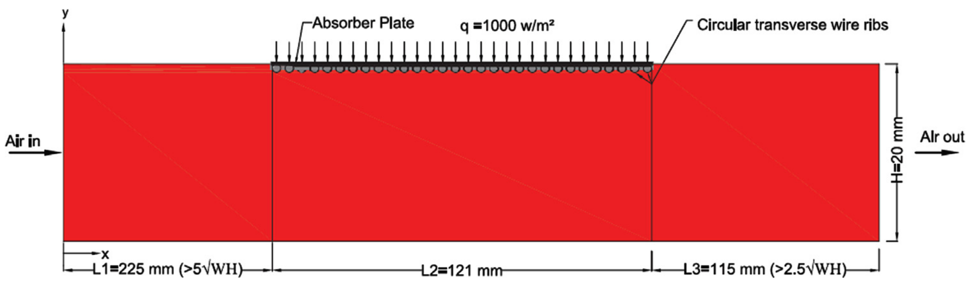


Fig. 71. Two dimensional domain for CFD analysis.

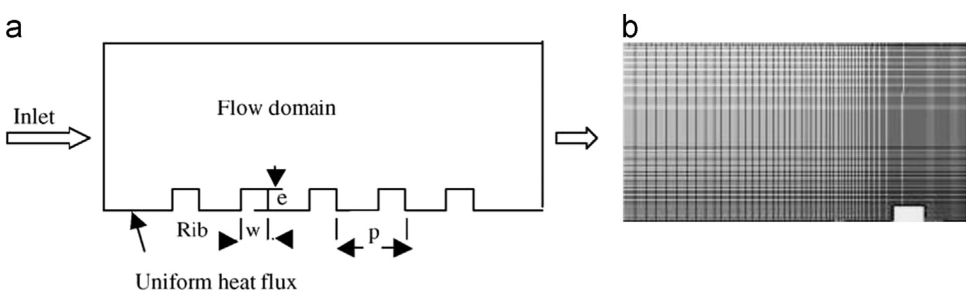


Fig. 72. (a) Ribbed duct geometry for CFD analysis and (b) two dimensional computational domain.

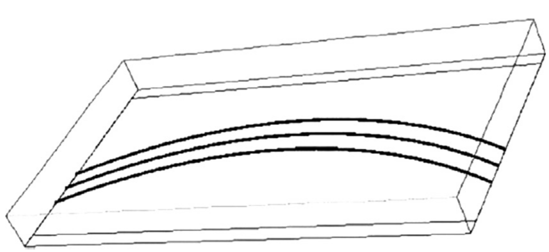


Fig. 73. Geometry of roughened surface collector plate.

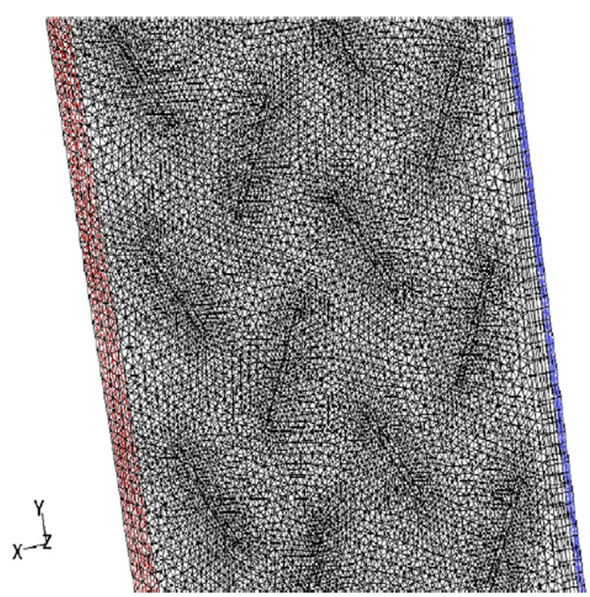


Fig. 74. Flow domain with 60° rib having circular cross section.

Karmare et al. [91] had carried out analysis using CFD on solar air heater with a absorber plate roughened with metal ribs of circular, square and triangular cross-section (Figs. 35 and 74), having 54°, 56°, 58°, 60° and 62° inclinations to the air flow. The system and operating parameters studied were: $e/D=0.044$, $P/e=17.5$ and $l/s=1.72$. Range of Reynolds number was 3600–17,000. Their study reported that maximum heat transfer is obtained with the square cross-section ribs with 58° angle of attack and there is 30% enhancement in the heat transfer for square plate over smooth surface.

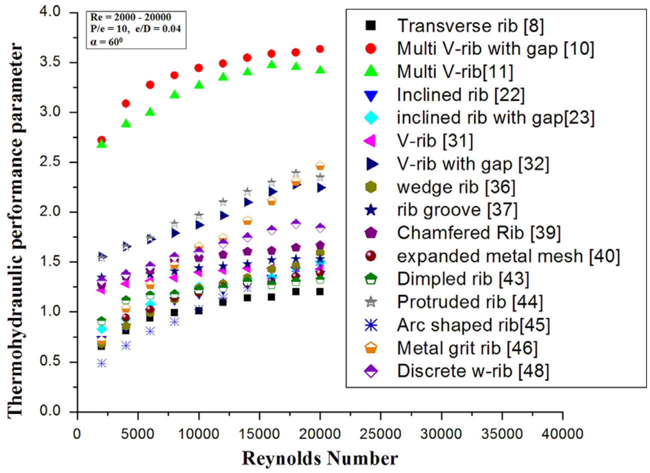


Fig. 75. Comparison of enhancement factor of different geometries.

The effect of wedge-shaped transverse ribs roughness on flow through a rectangular duct of a solar air heater is studied using CFD by Gandhi et al. [92]. Two dimensional CFD simulation is carried out using FLUENT on a duct having relative roughness pitch (P/e) of 4.5, relative roughness pitch of 0.022 and rib wedge angle of 15°. The results of numerical analysis are in good agreement with the experimental results in terms of velocity profile and turbulence intensity. The other observations revealed that rib roughened surface in a rectangular duct produced much flatter velocity profile and higher turbulence intensities as compared to smooth surface. This causes increase in heat transfer in roughened duct. Friction factor for roughened duct was around 3.4 times higher than the smooth duct at Reynolds number of 21,000.

CFD analysis on solar air heater is done by Sharma et al. [93] using V-shaped ribs roughness on the underside of the absorber plate. Finite volume method with semi-implicit method for pressure linked equations (SIMPLE) algorithm is used for computations. Reynolds number range was from 5000 to 15,000. The results obtained shows that combined effect of swirling motion, detachment and reattachment of the fluid were responsible for the increase of heat transfer rate during CFD analysis. Nusselt number increases and friction factor decreases with increase in Reynolds number for all combination of relative roughness height (e/D) and relative roughness pitch (P/e). An average percentage deviation predicted between CFD and exact solution was found less than ±3%. V-shaped rib roughness found to give high rate of heat transfer.

7. Comparison of thermo hydraulic performance of roughened solar air heaters

Various researchers reported that there is a heat transfer enhancement because of the inclusion of the roughness geometry in the path of the air flow. But this heat transfer enhancement is also leads to increased pumping power penalty due to corresponding increase in friction factor. So it is essential to determine the geometry that will results in the maximum enhancement in heat transfer and minimum increase in friction factor. This is done using a factor developed by Lewis [94] known as efficiency parameter, η which evaluates the enhancement of heat transfer for same pumping power requirement. It is defined as

$$\eta = (\mathrm{Nu_r}/\mathrm{Nu_s})/(f_r/f_s)^{1/3}$$

Correlations of heat transfer and friction factor for different roughness geometries are used to derive thermo hydraulic performance. Comparisons are made for the geometries having relative roughness pitch (P/e) value as 10 and relative roughness height
(e/D) value as 0.04. Range of Reynolds number is taken in between 2000 and 20,000. Thermo hydraulic performance parameter comparision of different types of ribs has been shown in Fig. 75. Following conclusions may be drawn from the figure

(1) Amongst all the roughness geometries considered for the comparison, Multi V-rib with a gap is found to give best thermohydraulic performance.
(2) The next best performance after multi V-rib with gap is achieved by V-rib as shown in Fig. 75.
(3) Other ribs are found to give thermo hydraulic performance in the range of 0.5 to 2.0.

8. Conclusions

In the present paper, an attempt has been made to review roughness geometries which have been used by researchers for the enhancement of heat transfer in solar air heater. It is found that substantial enhancement in the heat transfer can be achieved with little penalty of friction. In general the salient features of the reviews are

(1) Many investigators carried out number of experimental and numerical studies for better understanding of heat transfer enhancement and flow processes due to turbulence generated by the presence of roughness on absorber plate of a solar air heater. The paper presents a review of experimental as well as numerical analysis carried out by the researchers.
(2) The relative roughness height, relative roughness pitch, angle of attack and relative gap position are some of the parameters studied for their effect on heat transfer and friction characteristics in both heat exchangers and solar air heaters. The paper has given geometrical parameters for individual geometry, specifying the heat transfer enhancement in terms of Nusselt number and pressure drop penalty in terms of friction factor values.
(3) The application of solar air hater varies from industry to industry. Depending on the energy requirement, particular type of geometry can be selected. The reviews given in this paper may be useful in this regards.
(4) The heat transfer enhancement and friction factor characteristics in solar air heater are studied recently using Computational Fluid Dynamics (CFD) i.e. ANSYS-FLUENT software. CFD simulations results are found to be in good agreement with experimental results. The literature review on this area presented in this paper along with experimental work will be beneficial for the researchers working in simulation area using CFD.
(5) The correlations based on experimental results in the form of Nusselt number and friction factor are available in earlier papers which may be used to predict the thermal as well as thermo hydraulic performance of solar heaters. Heat transfer coefficient and friction factor correlations reported in the literature are presented in Table 1 which may be useful to the beginners for doing research in this area.
(6) Comparisons between various roughness geometries can be made on the basis of a parameter known as thermo hydraulic performance parameter (THPP). It is observed that multi V-rib with a gap gives better performance in comparison to others roughness geometries for Reynolds number range between 2000 and 20,000.

Table 1
Heat transfer coefficient and friction factor correlations for different roughness geometries used in solar air heater duct.

Investigators	Year	Roughness geometry	Range of parameters	Correlations	
				Heat transfer	Friction factor
Prasad and Saini [8]	1988	Transverse rib	e/D: 0.020–0.033 p/e: 10–20 Re: 5000–50,000	$S_t=(f/2)/[1+\sqrt{f/2\{4.5(e^+)^{0.28}\mathrm{Pr}^{0.57}-0.95(P/e)^{0.53}\}}]$	$f=2/[0.95(P/e)^{0.53}+2.5\ln(D/2e)-3.75]$
Lau et al [27]	1991	Combined rib (Transverse, inclined and V-shaped rib)	–	$G(e^+)=a(e^+)^b a=1.768-3.884 b=0.229-0.333$	$R(e^+)=a(e^+)^b a=0.968-2.269 b=0.055-0.152$
Hong and Hsieh [82]	1991	Transverse ribs	e/D_h: 0.19 p/e: 5.31	$Nu=0.056\mathrm{Re}_H{}^{0.74}\quad (for\ Tu=0.04)$ $Nu=0.030\mathrm{Re}_H{}^{0.79}\quad (for\ Tu=0.07)$ $Nu=0.019\mathrm{Re}_H{}^{0.83}\quad (for\ Tu=0.11)$	–
Gupta et al.[18]	1994	Transverse ribs	e/D: 0.018–0.052 Re: 3000–18,000	$Nu=0.000824(e/D)^{-0.178}(W/H)^{0.284}\mathrm{Re}^{1.062}\quad e\le 35$ $Nu=0.00307(e/D)^{-0.469}(W/H)^{0.245}\mathrm{Re}^{0.812}\quad e\ge 35$	$f=0.06412\,(e/D)^{0.019}(W/H)^{0.237}\mathrm{Re}^{-0.185}$
Gupta et al. [22]	1997	Inclined Ribs	e/D: 0.02–0.053 p/e: 7.5–10 α : 30–90° Re: 5000–30,000	$Nu=0.000824(e/D)^{-0.178}(W/H)^{0.284}\mathrm{Re}^{1.062}$ $\exp[-0.04(1-\alpha/60)^2](k/D)e\le 35$ $Nu=0.00307(e/D)^{-0.469}(W/H)^{0.245}\mathrm{Re}^{0.812}$ $\exp[-0.475(1-\alpha/60)^2](k/D)e\ge 35$	$f=0.06412(e/D)^{0.019}(W/H)^{0.237}\mathrm{Re}^{-0.185}$ $\exp[-0.0993(1-\alpha/60)^2]$
Saini and Saini [40]	1997	Expanded wire mesh metal ribs	l/e: 25–71.87 s/e: 15.62–46.87 e/D: 0.012–0.0390 Re: 1900–13,000	$\mathrm{Nu}=4.0\times 10^{-4}\mathrm{Re}^{1.22}(e/D)^{0.625}(s/10e)^{2.22}$ $\exp[-1.25\{\ln(s/10e)\}^2]\times(l/10e)^{2.66}$ $\times\exp[-0.824\{\ln(l/10e)^2\}]$	$f=0.815\mathrm{Re}^{0.361}(l/e)^{0.266}(s/10e)^{0.19}(10e/d)^{0.591}$
Muluwork et al.[33,34]	1998	V shaped staggered Discrete wire ribs	e/D: 0.02 α: 60° B/S: 3–9 Re: 2000–15,500	$\mathrm{Nu}=0.00534(B/S)^{1.3496}\mathrm{Re}^{1.2991}$	$f=0.7117(B/S)^{0.0636}\mathrm{Re}^{-2.991}$
Karwa et al. [39]	1999	Chamfered ribs	e/D: 0.014–0.0320 p/e: 4.5–8.5 Re: 3000–20,000 Φ: −15, 0, 10, 15, 18 W/H: 4.8, 6.1, 7.8, 9.66, 12	$G=103.77e^{-0.006}(W/H)^{0.5}(p/e)^{2.56}$ $\exp[0.7343\{\ln(p/e)\}^2](e^+)^{-0.31}$ for $7\le e^+\le 20$ $G=32.26e^{-0.006}(W/H)^{0.5}(p/e)^{2.56}$ $\exp[0.7343\{\ln(p/e)\}^2](e^+)^{0.8}$ for $20\le e^+\le 60$	for $7\le e^+\le 20$ $R=1.66e^{-0.0078}(W/H)^{-0.4}(p/e)^{2.695}$ $\exp[-0.762\{\ln(p/e)\}^2(e^+)^{-0.075}]$ for $20\le e^+\le 60$ $R=1.325e^{-0.0078}(W/H)^{-0.4}(p/e)^{2.695}$ $\exp[-0.762\{\ln(p/e)\}^2]$
Varma and Prasad [19]	2000	Transverse protrusion wire	e/D: 0.01–0.03 p/e: 10–40 Re: 5000–20,000 e^+: 8–42 P_r: 0.7	$\mathrm{Nu}=0.08596(p/e)^{-0.054}(e/D)^{0.072}\mathrm{Re}^{0.723}e\le 24$ $\mathrm{Nu}=0.0245(p/e)^{-0.016}(e/D)^{0.021}\mathrm{Re}^{0.802}e\ge 24$	$f=0.0245(p/e)^{-0.0206}(e/D)^{0.021}\mathrm{Re}^{-1.25}$
Momin et al.[31]	2002	V-shaped ribs	e/D: 0.02–0.034 p/e: 10 α: 30–90° Re: 2500–18,000	$\mathrm{Nu}=0.067(e/D)^{0.424}(\alpha/60)^{-0.077}\mathrm{Re}^{0.888}$ $\exp[-0.782\ln(\alpha/60)^2]$	$f=6.266(e/D)^{0.565}(\alpha/60)^{-0.093}\mathrm{Re}^{-0.425}$ $\exp[-0.719\ln(\alpha/60)^2]$
Bhagoria et al [36]	2002	Wedge shaped ribs	e/D: 0.015–0.033 p/e: 7.57 α: 8–15° Re: 3000–18,000	$\mathrm{Nu}=1.89\times 10^{-4}\mathrm{Re}^{1.21}(e/D)^{0.426}(p/e)^{2.94}(\phi/10)^{-0.018}$ $[\exp(-0.71(\ln(p/e))^2)][\exp(-1.50(\ln(\phi/10))^2)]$	$f=12.44(e/D)^{0.99}(\phi/10)^{0.49}\mathrm{Re}^{-0.18}(p/e)^{-0.52}$

Karwa [35]	2003	Inclined discrete and continuous wire ribs	e/D: 0.0467–0.05 p/e: 10 α: 60–90° B/S: 3 W/H: 7.19–7.75	$G=32.26e^{-0.006}(W/H)^{0.5}(p/e)^{2.56}$ $\exp[0.7343\{\ln(p/e)\}^2](e^+)^{-0.08}$	for $7\le e^+\le 20$ $R=1.66e^{-0.0078}(W/H)^{-0.4}(p/e)^{2.695}$ $\exp[-0.762\{\ln(p/e)\}^2(e^+)^{-0.075}]$ for $20\le e^+\le 60$ $R=1.325e^{-0.0078}(W/H)^{-0.4}(p/e)^{2.695}$ $\exp[-0.762\{\ln(p/e)\}^2]$
Jaurkeret al. [37]	2006	Rib-groove	e/D: 0.0181–0.0363 p/e: 4.5–10 g/p: 0.3–0.7 Re: 3000–21,000	$Nu=0.00206Re^{0.936}(e/D)^{0.349}(p/e)^{3.318}$ $\times\exp[-0.868\{\ln(p/e)\}^2](g/p)^{1.108}$ $\times\exp[2.486\{\ln(g/p)\}^2+1.405\{\ln(g/p)\}^3]$	$f=0.0012Re^{-0.199}(e/D)^{0.585}(p/e)^{7.19}$ $\times\exp[-1.854\{\ln(p/e)\}^2](g/p)^{0.645}$ $\times\exp[1.513\{\ln(g/p)\}^2+0.8662\{\ln(g/p)\}^3]$
Karmare and Tikewar [46]	2007	Metal grit rib	e/D: 0.035–0.044 p/e: 12.5–36 l/s: 1.72–1 Re: 4000–17,000	$Nu=2.4Re^{1/3}(e/D)^{0.42}(l/s)^{-0.146}(p/e)^{-0.27}$	$f=15.55Re^{-0.26}(e/D)^{0.94}(l/s)^{-0.27}(p/e)^{-0.51}$
Layek et al.[38]	2007	Chamfered rib groove combination	e/D: 0.022–0.04 p/e: 4.5–10 g/p: 0.3–0.6 Re: 3000–21,000	$Nu=0.002062Re^{0.936}(e/D)^{0.349}(p/e)^{3.318}$ $\exp[-0.868\{\ln(p/e)\}^2](g/p)^{1.108}$ $\times\exp[2.486\{\ln(g/p)\}^2+1.406\{\ln(g/p)\}^3]$	$f=0.001227Re^{-0.199}(e/D)^{0.585}(p/e)^{7.19}$ $\exp[-1.854\{\ln(p/e)\}^2](g/p)^{0.645}$ $\exp[1.513\{\ln(g/p)\}^2+0.8662\{\ln(g/p)\}^3]$
Saini and Verma [43]	2008	Dimple shaped protrusion	e/D: 0.018–0.037 p/e: 8–12 Re: 2000–12,000	$Nu=5.2\times10^{-4}Re^{1.27}(e/D)^{0.33}(p/e)^{3.15}$ $\exp[-2.21\{\ln(p/e)\}^2]\times\exp[-1.30\{\ln(e/D)\}^2]$	$f=0.0642Re^{-0.423}(e/D)^{-0.0214}(p/e)^{-0.465}$ $\exp[0.054\{\ln(p/e)\}^2]\exp[-0.840\{\ln(e/D)\}^2]$
Saini and Saini [45]	2008	Arc shaped wire ribs	e/D: 0.0213–0.0422 p/e: 10 g/e: 0.5–2 $\alpha/90$: 0.333–0.666 g/p: 0.3–0.6 Re: 2000–17,000	$Nu=0.001047(e/D)^{0.3772}(\alpha/90)^{-0.1198}Re^{1.3186}$	$f=0.14408(e/D)^{0.1765}(\alpha/90)^{0.1185}Re^{-0.17103}$
Kumar et al. [48]	2008	Discrete W shaped ribs	e/D: 0.0338 p/e: 10 ° α: 60	$Nu=0.105Re^{0.873}(e/D)^{0.453}(\alpha/60)^{-0.081}$ $\exp[-0.59\times(\ln(\alpha/60))^2]$	$f=5.68\times Re^{-0.40}(e/D)^{0.59}(\alpha/60)^{-0.081}$ $\exp[-0.579\times(\ln(\alpha/60))^2]$
Varun et al.[26]	2008	Inclined and transverse wire ribs	Re: 2000–14,000 p/e: 3–8	$Nu=0.0006(p/e)^{0.0104}Re^{1.213}$	$f=1.0858(p/e)^{0.0114}Re^{-0.3685}$
Bopche and Tandale [49]	2009	Inverted U shaped solid baffles	e/D: 0.0186–0.03986 p/e: 6.67–57.14 α: 90° Re: 3800–18,000	$Nu=0.5429Re^{0.7054}(e/D)^{0.3619}(p/e)^{-0.1592}$	$f=1.2134Re^{-0.2076}(e/D)^{0.3285}(p/e)^{-0.4259}$
Aharwal et al. [23]	2009	Inclined discrete ribs	e/D: 0.0377 p/e: 10 W/H: 5.87 d/w: 0.167–0.5 α: 60° Re: 3000–18,000	$Nu=0.0102Re^{1.148}(e/D)^{0.51}$ $[\{1-(0.25-d/w)^2(0.01(1-g/e)^2)\}]$	$f=0.5Re^{-0.0836}(e/D)^{0.72}$
Karwa et al. [69]	2009	Transverse perforated baffles	Re: 2700–11,150 p/e: 7.21, 14.42, 28.84 β: 26%, 46.8% δ/e: 0.047	$Nu=0.0893Re^{0.7608}$	$f=0.1673\ Re^{-0.0213}$
Hans et al. [11]	2010	Multiple V shaped	e/D: 0.019–0.043 p/e: 6–12 α: 30–75° Re: 2000–20,000 W/w: 1–10	$Nu=3.35\times10^{-5}Re^{0.92}(e/D)^{0.77}(W/w)^{0.43}(\alpha/90)^{-0.49}$ $\exp[-0.1177(\ln(W/w))^2]\exp[-0.61(\ln(\alpha/90))^2]$ $(p/e)^{8.54}\exp[-2.0407(\ln(p/e))^2]$	$f=4.47\times10^{-4}Re^{-0.3188}(e/D)^{0.73}(W/w)^{0.22}$ $(\alpha/90)^{-0.39}\exp[-0.52(\ln(\alpha/90))^2](p/e)^{8.9}$ $\exp[-2.133(\ln(p/e))^2]$

Table 1 (*continued*)

Investigators	Year	Roughness geometry	Range of parameters	Correlations	
				Heat transfer	Friction factor
Promvonge [55]	2010	Multiple 60° V shaped baffles	e/H:0.10, 0.20, 0.30 P/H: 1, 2, 3 Re: 5000–25,000	$\mathrm{Nu}=0.147\mathrm{Re}^{0.763}(PR)^{0.4}(1-e/H)^{-1.793}(1+PR)^{-0.42}$	$f=0.48\mathrm{Re}^{0.038}(1-e/H)^{-5.428}(1+PR)^{-0.833}$
Kumar et al. [25]	2011	60° inclined continuous discrete rib	Re: 4105.2–20,526.2 e/D: 0.0249, 0.0374 and 0.0498 p/e: 8, 12 and 16 d/W: 0.15, 0.25 and 0.35 g/e: 1	$\mathrm{Nu}=3\times10^{-5}\mathrm{Re}^{0.947}(e/D)^{0.290}(p/e)^{5.885}(d/W)^{0.115}$ $\exp[-1.237\{\ln(p/e)\}^2]$	$f=0.0014\mathrm{Re}^{-0.23}(e/D)^{0.804}(p/e)^{0.097}(p/e)^{4.516}$ $\exp[-0.944\{\ln(p/e)\}^2]$
Singh et al. [32]	2011	Discrete V-down ribs	Re: 3000–15,000 p/e: 4–12 α: 30–75° d/w: 0.2–0.8 g/e: 0.5–2.0 e/D: 0.015–0.043	$\mathrm{Nu}=2.36\times10^{-5}\mathrm{Re}^{0.90}(p/e)^{3.50}(\alpha/60)^{-0.023}(d/w)^{-0.043}$ $(g/e)^{-0.014}\exp[-0.84\{\ln(p/e)\}^2]\exp[-0.72\{\ln(\alpha/60)\}^2]$ $\exp[-0.05\{\ln(d/w)\}^2]\exp[-0.15\{\ln(g/e)\}^2]$	$f=44.13\times10^{-2}\mathrm{Re}^{-0.126}(p/e)^{2.74}(\alpha/60)^{-0.034}$ $(d/w)^{-0.058}(g/e)^{-0.031}(e/D)^{0.70}$ $\exp[-0.685\{\ln(p/e)\}^2]\exp[-0.93\{\ln(\alpha/60)\}^2]$ $\exp[-0.058\{\ln(d/w)\}^2]\exp[-0.21\{\ln(g/e)\}^2]$
Bhushan and Singh [44]	2011	Dimple Shape Roughness	S/e: 18.75–37.50 L/e: 25–37.5 d/D: 0.147–0.367 e/D: 0.03 Re: 4000–20,000	$\mathrm{Nu}=2.1\times10^{-88}\mathrm{Re}^{1.452}(S/e)^{12.94}(L/e)^{99.2}(d/D)^{-3.9}$ $\exp[-10.4\{\log(S/e)\}^2]\exp[-77.2\{\log(L/e)\}^2]$ $\exp[-7.83\{\ln(d/D)\}^2]$	$f=2.32\,\mathrm{Re}^{-0.201}(S/e)^{-0.383}(L/e)^{-0.484}(d/D)^{0.133}$
Lanjewar et al. [47]	2011	W-Shaped ribs	p/e: 10 e: 1.5 e/D: 0.03375 W/H: 8 Re: 2300–14,000 α: 30, 45, 60–75° e^+: 8–44	$R=\sqrt{(2/f)}+2.5\ln(2e/D)+3.75$ $e^+=\sqrt{(f/2)}\mathrm{Re}(e/D)$ $g=[(f/2St)-1]\sqrt{(2/f)}+R$	–
Yadav et al. [83]	2012	Circular protrusions	Re: 3600–18,100 p/e: 12–24 e/D: 0.015–0.03 α: 45–75 W/H: 11 e/d: 0.3	$\mathrm{Nu}=0.154\mathrm{Re}^{1.017}(p/e)^{-0.38}(e/D)^{0.521}(\alpha/60)^{-0.213}$ $\exp[-2.023\{\ln(\alpha/60)\}^2]$	$f=7.207\,\mathrm{Re}^{-0.56}(p/e)^{-0.18}(e/D)^{0.176}(\alpha/60)^{0.038}$ $\exp[1.412\{\ln(\alpha/60)\}^2]$
Sethi et al. [84]	2012	Angular fashion dimples	W/H: 11 e/D: 0.021–0.036 p/e: 10–20 α: 45–75° e/d: 0.5 Re: 3600–18,000	$\mathrm{Nu}=0.154\mathrm{Re}^{1.017}(p/e)^{-0.38}(e/D)^{0.521}(\alpha/60)^{-0.213}$ $\exp[-2.023\{\ln(\alpha/60)\}^2]$	$f=4.869\times10^{-1}\mathrm{Re}^{-0.223}(p/e)^{-0.059}(e/D)^{0.2663}(\alpha/60)^{0.0042}$ $\exp[-0.4801\{\ln(\alpha/60)\}^2]$
Chauhan et al [85]	2013	Impinging jets	Re: 3800–16,000 x/D_h: 0.435–1.739 y/D_h: 0.435–0.869 W/Z: 11.6 D_j/D_h: 0.045–0.109	$\mathrm{Nu}=1.658\times10^{-3}\mathrm{Re}^{0.8512}(X/D_h)^{0.1761}(Y/D_h)^{0.141}$ $(D_j/D_h)^{-1.9854}\exp[-0.3498\{\ln(D_j/D_h)\}^2]$	$f=0.3475\,\mathrm{Re}^{-0.5244}(X/D_h)^{0.4169}(Y/D_h)^{0.5321}$ $(D_j/D_h)^{-1.4848}\exp[-0.2210\{\ln(D_j/D_h)\}^2]$

References

[1] Ebrahim Momin Abdul-Malik, Saini JS, Solanki SC.. Heat transfer and friction in solar air heater duct with V-shaped rib roughness on absorber plate, vol. 45; 2002. p. 3383–3396.
[2] Varun, Saini RP, Singal SK. A review on roughness geometry used in solar air heaters. Solar Energy 2007;81:1340–50.
[3] Garg HP, Prakash J. Solar energy fundamentals and applications. New Delhi: Tata McGraw-Hill; 1997.
[4] Duffie JA, Beckman WA. Solar engineering of thermal processes. New York: Wiley; 1980.
[5] Frank K, Mark SB. Principles of heat transfer. Colorado: Thomson Learning Inc.; 2001.
[6] Patil AK, Saini JS, Kumar K. A comprehensive review on roughness geometries and ınvestigation techniques used in artificially roughened solar air heaters. Int J Renewable Energy Res 2012;2(1).
[7] Prasad BN, Saini JS. Optimal thermo hydraulic performance of artificially roughened solar air heaters. Sol Energy 1991;47:91–6.
[8] Prasad BN, Saini JS. Effect of artificial roughness on heat transfer and friction factor in a solar air heater. Sol Energy 1988;41:555–60.
[9] Taslim ME, Li T, Kretcher DM. Experimental heat transfer and friction in channels roughened with angled, v-shaped and discrete ribs on two opposite walls. Trans ASME J Turbomach 1996;118:20–8.
[10] Kumar Anil, Saini RP, Saini JS. Experimental investigation on heat transfer and fluid flowcharacteristics of air flow in a rectangular duct with Multi v-shaped rib with gap roughness on the heated plate 2012:1733–49.
[11] Hans VS, Saini RP, Saini JS. Heat transfer and friction factor correlations for a solar air heater duct roughened artificially with multiple v-ribs. Sol Energy 2010;84:898–911.
[12] Aharwal KR, Gandhi BK, Saini JS. Experimental investigation on heat-transfer enhancement due to a gap in an inclined continuous rib arrangement in a rectangular duct of solar air heater. Renew Energy 2008;33:585–96.
[13] Muluwork KB. Investigations on fluid flow and heat transfer in roughened absorber solar heaters [Ph.D. dissertation]. IIT, Roorkee-247667, India; 2000.
[14] Sparrow EM, Hossfeld LM. Effect of rounding of protruding edges on heat transfer and pressure drop in a duct. Int J Heat Mass Transfer 1984;27:1715–23.
[15] Prasad K, Mullick SC. Heat transfer characteristics of a solar air heater used for drying purposes. Appl Energy 1983;13(2):83–93.
[16] Prasad BN, Saini JS. Effect of artificial roughness on heat transfer and friction factor in a solar air heater. Sol Energy 1988;41(6):555–60.
[17] Kays WB. Convective heat and mass transfer. New York: McGraw Hill Book Co.; 1966; 197–8.
[18] Gupta D, Solanki SC, Saini JS. Heat and fluid flow in rectangular solar air heater ducts having transverse rib roughness on absorber plates. Sol Energy 1993;51 (1):31–7.
[19] Verma SK, Prasad BN. Investigation for the optimal thermo hydraulic performance of artificially roughened solar air heaters. Renew Energy 2000;20:19–36.
[20] Sahu MM, Bhagoria JL. Augmentation of heat transfer coefficient by using 90° broken transverse ribs on absorber plate of solar air heater. Renew Energy 2005;30:2063–75.
[21] Han JC, Park CK. Augmented heat transfer in rectangular channels of narrow aspect ratios with rib turbulators. Int J Heat Mass Trans 1989;32:1619–30.
[22] Gupta D, Solanki SC, Saini JS. Thermo hydraulic performance of solar air heaters with roughened absorber plates. Sol Energy 1997;61:33–42.
[23] Aharwal KR, Gandhi BK, Saini JS. Experimental investigation on heat-transfer enhancement due to a gap in an inclined continuous rib arrangement in a rectangular duct of solar air heater. Renew Energy 2008;33:585–96.
[24] Cho HH, Kim YY, Rhee DH, Lee SY. The effect of gap position in discrete ribs on local heat/mass transfer in a square duct. J Enhanced Heat Trans 2003;10:287–300.
[25] Kumar ST, Mittal V, Thakur NS, Kumar A. Heat transfer and friction factor correlations for rectangular solar air heater duct having 60° inclined continuous discrete rib arrangement. Br J Appl Sci Technol 2011;3:67–93.
[26] Varun, Saini RP, Singal SK. Investigation of thermal performance of solar air heater having roughness elements as a combination of inclined and transverse ribs on the absorber plate. Renew Energy 2008;33:1398–405.
[27] Lau SC, Kukraja RT, McMillin RD. Effect of V-shaped rib arrays on turbulent heat transfer and friction of fully developed flow in a square channel. Int J Heat Mass Transfer 1991;34:1605–16.
[28] Lau SC, McMillin RD, Han JC. Heat transfer characteristics of turbulent flow in a square channel with angle discrete ribs. ASME J Turbomach 1991;113:367–74.
[29] Lau SC, McMillin RD, Han JC. Turbulent heat transfer and friction in a square channel with discrete rib turbulators. ASME J Turbomach 1991;113:360–6.
[30] Han JC, Zhang YM, Lee CP. Augmented heat transfer in square channels with parallel, crossed and V-shaped angled ribs. Trans ASME J Heat Transf 1991;113:590–6.
[31] Momin AME, Saini JS, Solanki SC. Heat transfer and friction in solar air heater duct with v-shaped rib roughness on absorber plate. Int J Heat Mass Transf 2002;45:3383–96.
[32] Singh S, Chander S, Saini JS. Heat transfer and friction factor correlations of solar air heater ducts artificially roughened with discrete V-down ribs. Energy 2011;36:5053–64.
[33] Muluwork KB, Saini JS, Solanki SC. Studies on discrete rib roughened solar air heaters. In: Proceedings of national solar energy convention; 1998. p. 75–84.
[34] Muluwork KB. Investigations on fluid flow and heat transfer in roughened absorber solar heaters [Ph.D. thesis]. IIT, Roorkee; 2000.
[35] Karwa R. Experimental studies of augmented heat transfer and friction in asymmetrically heated rectangular ducts with ribs on the heated wall in transverse, inclined, v-continuous and v-discrete pattern. Int Commun Heat Mass Transf 2003;30:241–50.
[36] Bhagoria JL, Saini JS, Solanki SC. Heat transfer coefficient and friction factor correlations for rectangular solar air heater duct having transverse wedge shaped rib roughness on the absorber plate. Renew Energy 2002;25:341–69.
[37] Jaurker AR, Saini JS, Gandhi BK. Heat transfer and friction characteristics of rectangular solar air heater duct using rib-grooved artificial roughness. Sol Energy 2006;80(8):895–907.
[38] Layek A, Saini JS, Solanki SC. Second law optimization of a solar air heater having chamfered rib-groove roughness on absorber plate. Renew Energy 2007;32:1967–80.
[39] Karwa R, Solanki SC, Saini JS. Heat transfer coefficient and friction factor correlations for the transitional flow regime in rib-roughened rectangular ducts. Int J Heat Mass Transf 1999;42:1597–615.
[40] Saini RP, Saini JS. Heat transfer and friction factor correlations for artificially roughened ducts with expanded metal mesh as roughened element. Int J Heat Mass Transf 1997;40:973–86.
[41] Gupta MK, Kaushik SC. Performance evaluation of solar air heater having expanded metal mesh as artificial roughness on absorber plate. Int J Therm Sci 2009;48:1007–16.
[42] Paswan MK, Sharma SP. Thermal performance of wire-mesh roughened solar air heaters. Arab Res Inst Sci Eng 2009;1:31–40pp 2009;1:31–40.
[43] Saini RP, Verma J. Heat transfer and friction factor correlations for a duct having dimple-shaped artificial roughness for solar air heaters. Energy 2008;133:1277–87.
[44] Bhushan B, Singh R. Nusselt number and friction factor correlations for solar air heater duct having artificially roughened absorber plate. Sol Energy 2011;85:1109–18.
[45] Saini SK, Saini RP. Development of correlations for Nusselt number and friction factor for solar air heater with roughened duct having arc-shaped wire as artificial roughness. Sol Energy 2008;82:1118–3110.
[46] Karmare SV, Tikekar AN. Heat transfer and friction factor correlation for artificially roughened duct with metal grit ribs. Int J Heat Mass Transf 2007;50:4342–51.
[47] Lanjewar A, Bhagoria JL, Sarviya RM. Experimental study of augmented heat transfer and friction in solar air heater with different orientations of w-rib roughness. Exp Therm Fluid Sci 2011;35:986–95.
[48] Kumar A, Bhagoria JL, Sarviya RM. International 19th national & 8th ISHMT-ASME heat and mass transfer conference heat transfer enhancement in channel of solar air collector by using discrete w-shaped artificial roughened absorber; 2008.
[49] Bopche SB, Tandale MS. Experimental investigation on heat transfer and frictional characteristics of a turbulator roughened solar air heater duct. Int J Heat Mass Transf 2009;52:2834–48.
[50] Sriromreun P, Promvong P. Augmented heat transfer in rectangular duct with angled Z-shaped ribs. In: Proceedings of the ınternational conference on energy and sustainable development, Thailand; 2–4 June, 2010.
[51] Yeh HM, Chou WH. Efficiency of solar air heaters with baffles. Energy 1991;16:983–7.
[52] Yeh HM, Ho CD, Lin CY. The influence of collector aspect ratio on the collector efficiency of baffled solar air heaters. Energy 1998;23:11–6.
[53] Sripattanapipat S, Promvonge P. Numerical analysis of laminar heat transfer in a channel with diamond shaped baffles. Int Commun Heat Mass Transf 2009;36:32–8.
[54] Nie JH, Chen YT, Hsieh HT. Effects of a baffle on separated convection flow adjacent to backward facing step. Int J Therm Sci 2009;48:618–25.
[55] Promvonge P. Heat transfer and pressure drop in a channel with multiple 60°V baffles. Int Commun Heat Mass Transf 2010;37:835–40.
[56] Promvonge P, Jedsadaratanachai W, Kwankaomeng S. Numerical study of laminar flow and heat transfer in square channel with 30° inline angled baffle turbulators. Appl Therm Eng 2010;30:1292–303.
[57] Kwankaomeng S, Promvonge P. Numerical prediction on laminar heat transfer in square duct with 30° angled baffle on one wall. Int Commun Heat Mass Transf 2010;37:857–66.
[58] Promvonge P, Kwankaomeng S. Periodic laminar flow and heat transfer in a channel with 45° staggered V baffles. Int Commun Heat Mass Transf 2010;37:841–9.
[59] Promvonge P, Jedsadaratanachai W, Kwankaomeng S, Thianpong C. 3D simulation of laminar flow and heat transfer in V-baffled square channel. Int Commun Heat Mass Transf 2012;39:85–93.
[60] Promvonge P, Sripattanapipat S, Kwankaomeng S. Laminar periodic flow and heat transfer in square channel with 45° inline baffles on two opposite walls. Int J Therm Sci 2010;49:963–75.
[61] Kwankaomeng S, Jedsadaratanachai W, Promvonge P. Laminar periodic flow and heat transfer in square channel with 30° ınclined baffles, PEA-AIT ınternational conference on energy and sustainable development: ıssues and strategies (ESD 2010).The Empress Hotel, Chiang Mai, Thailand; 2–4 June 2010.
[62] Ho Chii-Dong, Chang H, Rei-Chi Wang, Lin Chun-Sheng. Performance improvement of a double-pass solar air heater with fins and baffles under recycling operation. Appl Energy 2012.
[63] Sriromreun P, Thianpong C, Promvonge P. Experimental and numerical study on heat transfer enhancement in a channel with Z-shaped baffles. Int Commun Heat Mass Transf 2012;39:945–52.

[64] Yang YT, Hwang CZ. Calculation of turbulent flow and heat transfer in a porous baffled channel. Int J Heat Mass Transf 2003;46:771–80.
[65] Ko KH, Anand NK. Use of porous baffles to enhance heat transfer in a rectangular channel. Int J Heat Mass Transf 2003;46:4191–9.
[66] Tzeng SC, Jeng TM, Wang YC. Experimental study of forced convection in asymmetrically heated sintered porous channels with/without periodic baffles. Int J Heat Mass Transf 2006;49:78–88.
[67] Lin CW. Experimental study of thermal behaviors in a rectangular channel with baffle of pores. Int Commun Heat Mass Transf 2006;33:985–92.
[68] Huang KD, Tzeng SC, Jeng TM, Wang JR, Cheng SY, Tseng KT. Experimental study of fluid flow and heat transfer characteristics in the square channel with a perforation baffle. Int Commun Heat Mass Transf 2008;35:1106–12.
[69] Karwa R, Maheshwari BK. Heat transfer and friction in an asymmetrically heated rectangular duct with half and fully perforated baffles at different pitches. Int Commun Heat Mass Transf 2009;36:264–8.
[70] Gentry MC, Jacobi AM. Heat transfer enhancement by delta-wing vortex generators on a flat plate: vortex interactions with the boundary layer. Exp Therm Fluid Sci 1997;14:231–42.
[71] Torii K, Kwak KM, Nishino K. Heat transfer enhancement accompanying pressure loss reduction with winglet type vortex generators for fin tube heat exchangers. Int J Heat Mass Transf 2002;45:3795–801.
[72] Yakut K, Sahin B, Celik C, Alemdaroglu N, Kurnuc A. Effect of tapes with double sided delta winglets on heat and vortex characteristics. Appl Energy 2005;80:77–95.
[73] Joardar A, Jacobi AM. Heat transfer enhancement by winglet type vortex generator arrays in compact plain fin and tube heat exchanger. Int J Refrig 2008;31:87–97.
[74] Tian L, He Y, Tao Y, Tao W. A comparative study on the air side performance of wavy fin and tube heat exchanger with punched delta winglets in staggered and inline arrangements. Int J Therm Sci 2009;48:1765–76.
[75] Min C, Qi C, Kong X, Dong J. Experimental study of rectangular channel with modified rectangular longitudinal vortex generators. Int J Heat Mass Transf 2010;53:3023–9.
[76] Kotcioglu I, Caliskan S, Cansiz A, Baskaya S. Second law analysis and heat transfer in a cross flow heat exchanger with a new winglet type vortex generator. Energy 2010;35:3686–95.
[77] Eiamsa-ard S, Wongcharee K, Eiamsa-ard P, Thianpong C. Heat transfer enhancement in a tube using delta winglet twisted tapes inserts. Appl Therm Eng 2010;30:310–8.
[78] Chompookham T, Thianpong C, Kwankaomeng S, Promvonge P. Heat transfer augmentation in a wedge ribbed channel using winglet vortex generators. Int Commun Heat Mass Transf 2010;37:163–9.
[79] Promvonge P, Khanoknaiyakarn C, Kwankaomeng S, Thianpong C. Thermal behavior in solar air heater channel fitted with combined rib and delta winglet. Int Commun Heat Mass Transf 2011;38:749–56.
[80] Zhou G, Ye Q. Experimental investigations of thermal and flow characteristics of curved trapezoidal winglet type vortex generators. Appl Therm Eng 2012;37:241–8.
[81] Tanda G. Effect of rib spacing on heat transfer and friction in a rectangular channel with 45° angled rib turbulators on one/two walls. Int J Heat Mass Transf 2011;54:1081–90.
[82] Hong YJ, Hsieh SS. An experimental investigation of heat transfer characteristics for turbulent flow over staggered ribs in a square duct. Exp Therm Fluid Sci 1991;4:714–22.
[83] Yadav S., Maneesh Kaushal, Varun, Siddhartha. Nusselt number and friction factor correlations for solar air heater duct having protrusions as roughness elements on absorber plate; 2012.
[84] Sethi M, Varun, Thakur NS. Correlations for solar air heater duct with dimpled shape roughness elements on absorber plate. Sol Energy 2012;86:2852–61.
[85] Chauhan R, Thakur NS. Heat transfer and friction factor correlations for impinging jet solar air heater. Exp Therm Fluid Sci 2013;44:760–7.
[86] Yadav AS, Bhagoria JL. Modeling and simulation of turbulent flows through a solar air heater having square-sectioned transverse rib roughness on the absorber plate. Sci World J 2013.
[87] Yadav AS, Bhagoria JL. Numerical investigation of flow through an artificially roughened solar air heater. Int J Ambient Energy 2013.
[88] Yadav AS, Bhagoria JL. A CFD (computational fluid dynamics) based heat transfer and fluid flow analysis of a solar air heater provided with circular transverse wire rib roughness on the absorber plate. Energy 2013;55:1127–42.
[89] Chaube A, Sahoo PK, Solanki SC. Analysis of heat transfer augmentation and flow characteristics due to rib roughness over absorber plate of a solar air heater. Renew Energy 2006;31(3):317–31.
[90] Kumar S, Saini RP. CFD based performance analysis of a solar air heater duct provided with artificial roughness. Renew Energy 2009;34:1285–91.
[91] Karmare SV, Tikekar AN. Analysis of fluid flow and heat transfer in a rib grit roughened surface solar air heater using CFD. Sol Energy 2010;84(3):409–17.
[92] Gandhi BK, Singh KM. Experimental and numerical ınvestigations on flow through wedge shape rib roughened duct. Inst Eng (India) J-MC 2010;90:13–8.
[93] Sharma AK, Thakur NS. CFD based fluid flow and heat transfer analysis of a v-shaped roughened surface solar air heater. Int J Eng Sci Technol 2012;4(5):2115–21.
[94] Lewis MJ. Optimizing the thermohydraulic performance of rough surfaces. Int J Heat Mass Tranasf 1975;181243e8 1975;18.